Deanship of Graduate Studies
Al – Quds University

Effect of Rare Earth Ion Size on Ordering Processes in Rare Earth Ferrites RFe_2O_4 by $R=Lu_xY_{1-x}Fe_2O_4$ Substitution Study

Sabreen Saleh Said Hammouda

M.Sc. Thesis

Jerusalem-Palestine

1437/2016

Effect of Rare Earth Ion Size on Ordering Processes in Rare Earth Ferrites RFe_2O_4 by $R=Lu_xY_{1-x}Fe_2O_4$ Substitution Study

Prepared By:

Sabreen Saleh Said Hammouda

B.SC. physics science Al-Quds University- Palestine

Supervisors

Prof. Salman M. Salman
Physics Department, Al-Quds University, Palestine

Prof. Manuel Angst
Jülich Centre for Neutron Science institute (JCNS-2), Jülich Research Center, Germany

A thesis submitted in partial fulfillment of requirement for the degree of Master of Science in Physics

1437/2016

Al – Quds University

Deanship of Graduate Studies

Department of Physics

Thesis Approval

Effect of Rare Earth Ion Size on Ordering Processes in Rare Earth Ferrites RFe_2O_4 by $R=Lu_xY_{1-x}Fe_2O_4$ Substitution Study

Sabreen Saleh Said Hammouda

Registration No: 21220338

Supervisors:

Prof. Salman M Salman, Physics Al-Quds University, Palestine.

Prof. Manuel Angst, Jülich Centre for Neutron Science Institute (JCNS-2), FZ Jülich, Germany.

Master thesis submitted and accepted: 3/1/2016

Names and signatures of examining committee members:

1. Head of the committee: Prof. Salman M Salman Signature:
2. Internal Examiner: Prof. Saqer Darweesh Signature:
3. External Examiner: Prof. Mustafa Abu Safa Signature:

Jerusalem- Palestine
1437/2016

Dedication

I lovingly dedicate this research to

The Sake of Allah.
My homeland, the bleeding Palestine, and it's capital, my beloved Jerusalem, and the memory of martyrs.

To my great parents for their endless love.
My beloved brothers and sisters, specially my dearest sister, Manal.
My dear uncle, Abdul Qavi, who guided me by his wisdom and unlimited support during all stages of my study.
To my extended family, the symbol of love and giving.
My friends everywhere who encouraged and supported me.

Declaration

I, Sabreen S. Hammouda, declare that this thesis **"Effect of rare earth ion size on ordering processes in rare earth ferrites RFe_2O_4 by $R=Lu_xY_{1-x}Fe_2O_4$ substitution study"** and the work presented in it are my own and have been generated by me as the result of my own original research and that they have not been submitted earlier elsewhere.

I confirm that this work was done under the supervision of Professor Salman M. Salman from the Physics Department, Al-Quds University, Palestine, and Prof. Manuel Angst from the Jülich Centre for Neutron Science (JCNS-2), Forschungszentrum Jülich, Germany*.

Sign:

Sabreen S. Hammouda

Date: 3/1/2016

The project is part of a collaborative effort under the under the SCP-2 of the framework collaboration between the Forschungszentrum Jülich Germany, and al-Quds University, Palestine, and coordinated by Professors Thomas Brückel Director from JCNS, and Salman M. Salman from Physics and Director of Al-Quds Jülich Cooperation Program at Al-Quds University.

Acknowledgements

First, I am grateful to **Allah** for giving me the strength to complete this work.

I would like to thank my Advisor **Prof. Salman M. Salman** for his guidance during my university studies and providing the chance to conduct this experiment within the framework of Alquds Jülich Cooperation.

I like to express my thanks to **Prof. Thomas Brückel** for providing the support and hospitality to conduct my thesis at the wonderful JCNS-2 institute.

I extend my gratitude to my supervisor **Prof. Manuel Angst** for his patience, motivation, knowledge, and the fruitful discussions and valuable guidance that helped me during the experiment and writing this manuscript.

I was always proud to be a member of the great group: **Pankaj Thakuria**, **Giorgi Khazaradze**, **Hailey Williamson, and Thomas Müller** with whom I cannot imagine having a better tutor. He was always helpful whenever I faced problems. Thank you.

Special thanks to **Miss Barbara Köppchen** for her steady support in all administrative matters including travel and support. Thank you **Mr. Jörg Persson** for your help during my work in the ceramic lab and to **Mr. Jochen Friedrich** for doing the TGA measurements. Special thanks go to **Dr. Buad Khales,** for her encouragement, and being a true sister.

Special appreciation for the constant support of my uncle **Mr. Abdul Qavi** without which I may not have finished my graduate studies. Thanks to my ant **Nehad Hushia** for her care. I am truly thankful to **Miss Jessi and her spouse Dr. Mazen Qumsiyeh**.

I take this opportunity to thank **my teachers and professors** in all stages of my studies. You all were candles that lightened my way. Thanks to all people who stood beside me and left their imprint on my life.

Sabreen S. Hammouda

Abstract

Rare earth ferrites RFe_2O_4 have attracted a lot of attention as prototypical examples of Multiferroics, which have a potential use in information technology in particular due to their proposed new mechanism of ferroelectricity arising from charge ordering (CO). The aim of this thesis is to elucidate the evolution of charge and spin order as a function of the rare earth ion size. This is done by a partial substitution study, i.e. the investigation of $Lu_xY_{1-x}Fe_2O_4$. $YbFe_2O_4$ exhibits a behavior very similar to $LuFe_2O_4$, consistent with the primary importance of the rare earth ion size, which is comparable for both Yb^{3+} and Lu^{3+}.

Alternatively, the Y^{3+} ionic radius is much larger, and a completely different charge order was found. The critical aspect of this study was that, for each substitution level x, the oxygen-stoichiometry was fine-tuned, because O-stoichiometry, variations effects are hard to distinguish neatly from the rare earth substitutions. To tune the oxygen-stoichiometry, the synthesis of polycrystalline $Lu_xY_{1-x}Fe_2O_4$ (x = 0.5, 0.1) was done under a CO_2-H_2 (4%)/Ar (96%) gas flow, and the single crystals were grown by an image furnace under a tunable flow of CO:CO_2 to control the oxygen partial pressure. The charge order was investigated in-house with the single-crystal X-ray diffraction (XRD).

The characterization of the magnetic properties on the polycrystalline $Lu_{0.5}Y_{0.5}Fe_2O_4$ implies different magnetic behaviors for different stoichiometry levels. A best quality polycrystalline sample was obtained exhibiting a sharp peak transition at ~240 K, with large thermal hysterics. A first order meta-magnetic transition triggering a competition between antiferromagnetic (AFM) and ferrimagnetic (fM) phases was possibly observed in isothermal M (H) measurements conducted on the best polycrystalline sample, and confirming the magnetic behavior similarities with $LuFe_2O_4$.

For all the grown crystals, the magnetic behavior generally was not as good as for the polycrystalline samples. The X-ray diffraction showed 2D charge order with diffuse scattering along (1/3 1/3 ℓ) at different temperatures indicating that the crystals are not stoichiometric enough. The few prepared polycrystalline $Lu_{0.1}Y_{0.9}Fe_2O_{4-\delta}$ samples exhibited a different magnetic behavior from that of YFe_2O_4, $Lu_{0.5}Y_{0.5}Fe_2O_4$ and Kishi's sample. However, the comparisons are tentative, since no stoichiometric samples were available. It is quite important to prove that and explain why this high percentage Y phase has different charge and spin orders compared to both $LuFe_2O_4$ and YFe_2O_4.

Contents **page**

List of Tables

List of Figures

List of Abbreviations

ME	Magneto-electric
S	Spin
Δρ	Charge
M	Magnetization
E	Electric field
H	Magnetic field
P	Polarization
MRAM	Magnetic Random Access Memory
GMR	Giant Magneto-Resistance
RAM	Random Access Memory
FE	Ferroelectric
AFM	Antiferromagnetic
V	Voltage
R	Resistance
CO	Charge Order
BVS	Bond-Valence-Sum
XMCD	X-ray Magnetic Circular Dichroism
DFT	Density-Functional-Theory
δ	oxygen deficiency.
ZFC	Zero Field Cooling
FC	Field Cooling
FW	Field Warming
FZ	Floating Zone
XRD	X-ray diffraction
JCNS	Jülich Center for Neutron Science
OFZ	Optical Floating Zone
k	Wave vector
Q	scattering vector
d	Plane spacing
λ	wavelength
VSM	Vibrating Sample Magnetometer
PPMS	Physical Properties Measurement System
ICSD	International Crystallographic Database
TGA	Thermo-Gravimetric-Analysis
fM	ferrimagnetic
RT	Room temperature
f.u.	formula unit

1 *Introduction*

1.1 Introduction

Transition metal oxides are examples of correlated electron systems and form a very active research field due to their intrinsic complexity arising from the interplay of many active degrees of freedom–charge, spin, orbital and lattice, which can lead to functionalities, with potential applications (e.g. colossal magnetoresistance **[Volger, 1954]** and multi-ferroicity **[Fiebig, 2005], [Eerenstein et al., 2006] and [Schmid, 2008]**). Moreover, "geometrical frustration" **[Moessner and Ramirez, 2006]**, in which a crystal structure with e.g. triangular arrangements (illustrated in Figure 1.1) leads to competition between different interactions, produces complex possible ground states further facilitating interesting functionalities.

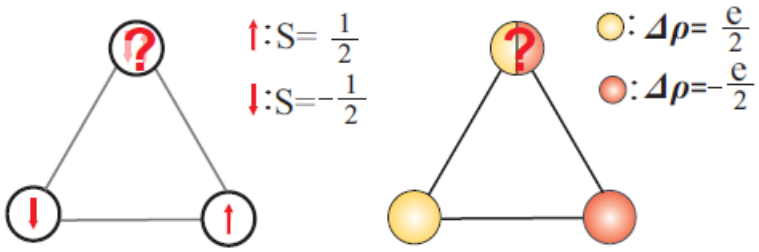

Figure 1.1 Spin and charge frustration on a triangular lattice. On a triangle with antiferromagnetic interactions, two of the spins are aligned antiparallel, the third one cannot align opposite to both other spins and creates geometric magnetic frustration. The same principle works for charge ordering. Taken from [de Groot, 2012].

Multiferroics build a class of multifunctional materials, which exhibit multiple ferroic orders in a single phase. Ferroic ordering is actually found in a material, which has a spontaneous long range order below a certain critical temperature, that can be ferroelectricity, (anti-)ferromagnetism, and spontaneous deformation.

In particular, materials combining magnetism and ferroelectricity (termed as Multiferroics) **[Khomskii, 2009]** may display large magnetoelectric (ME) coupling which offers a promising approach for the future of information technology, because this interplay enables the

control of the ferroelectric polarization by a magnetic field and conversely the control of the magnetization by an electric field, see figure 1.2. Therefore, new device functions are likely to emerge.

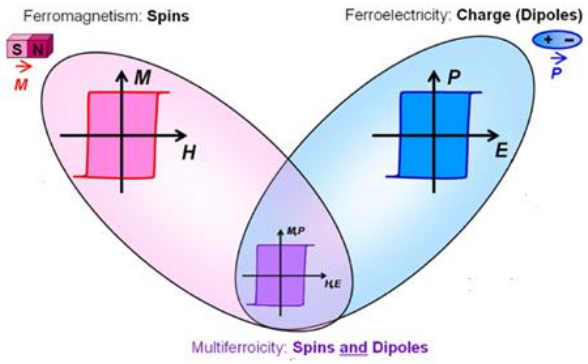

Figure 1.2 ME Multiferroics combine both ferroelectricity and magnetism represented by the overlapping area, the coupling between these orders leads to a ferroelectric response to a magnetic field and vice versa. Taken from [de Groot, 2012].

A technological motivation examples are, Magnetic Random Access Memories (MRAM), in which the information is encoded as binary bit in the parallel (0) or antiparallel (1) alignment of the magnetization of two layers and read out with the Giant Magneto-Resistance (GMR) effect **[41st IFF Spring school, 2010]**.

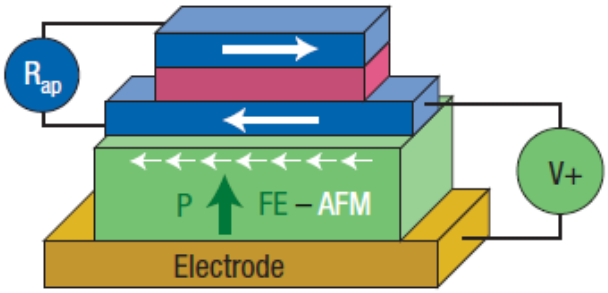

Figure 1.3 Multiferroics RAM. The information is stored by the magnetization of the two blue layers and is read out by GMR, but with the insertion of a Multiferroics (green) layer, the information is stored by applying a voltage. Taken from [Bibes and Barthélémy, 2008].

The main problem of this storage media is the high power consumption, because the writing process needs significant current to re-magnetize the layer. To overcome this problem, one could insert a layer of an (insulating) Multiferroics-material with strong magneto electric coupling, so the information can be written by applying a voltage i.e. convert a voltage to a magnetization **[Bibes and Barthélémy, 2008].** Multiferroics RAM is sketched in figure 1.3. Antiferromagnetic (AFM) ferroelectric materials can be used as insulating layers as

well by employing the exchange bias effect **[Yoshii et al., 2012] and [Roy et al., 2012]**. The GMR was discovered by Albert Fer and Peter Grünberg in 1988, (Physics Noble Price 2007).

Unfortunately, ME Multiferroics materials, are rare **[Hill, 2000]**, because the traditional mechanism of ferroelectricity is incompatible with magnetism. For example, the symmetry break leading to ferroelectricity in $BaTiO_3$ is achieved by off-center displacement of the transition metal ion Ti^{4+}. The Ti-ion is at the center of the oxygen octahedral cage as shown in figure 1.4, i.e. the d-orbital of Ti^{4+} pointing to the p-orbital of oxygen. Therefore, one of the O_p filled by two electrons makes bonding and antibonding molecular orbitals that are capable of holding 2e-.

For an empty d shell, only the bonding orbital is occupied by 2e- of oxygen, but for a non-empty d shell, the antibonding orbital will be occupied by an extra electron of d leading **[41st IFF Spring school, 2010]**. Therefore, the ferroelectricity of $BaTiO_3$ requires an empty d shell, but magnetism requires unpaired d electrons. Magnetism and ferroelectricity thus seem to exclude each other. In addition, a symmetry issue is noticed in ME Multiferroics: ferroelectric order can only exist in a material with broken inversion symmetry, while ferromagnetism exists in a material with broken time-reversal symmetry, therefore multiferroicity can only occur in materials with violation of both **[Schmid, 2008]**. Subsequently, this scarcity enlightens us to focus on alternative mechanisms of ferroelectricity, one of these is multi-ferroicity due to charge ordering.

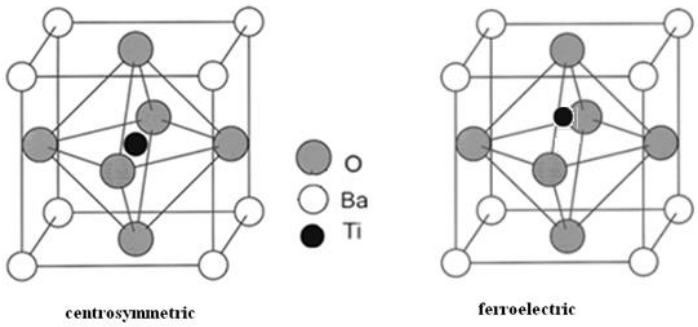

Figure 1.4 Traditional mechanism of ferroelectricity in $BaTiO_3$, off center displacement of Ti ion to drive ferroelectricity. Left side figure taken from [Hill, 2000].

1.1.1 Multi-ferroicity due to charge ordering

Polarization occurs when electric dipoles, which are equal charges of opposite polarity separated by a distance, break the inversion symmetry. Figure (1.5a), shows a chain of periodic opposite equal charges in a centrosymmetric fashion, which results in a zero net dipole moment i.e. $\Sigma P=0$, whereas if these charges are arranged in a non-centrosymmetric fashion illustrated in figure (1.5b), a net polarization is developed i.e. $\Sigma P\neq 0$, which indeed induces ferroelectricity.

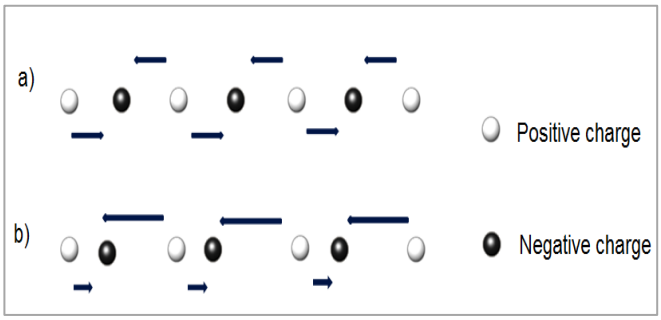

Figure 1.5 a) Centrosymmetric charge ordering, with no net polarization. b) Non centrosymmetric charge ordering, with a net polarization. Reproduced from [van den Brink and Khomskii, 2008].

The appearance of charge order (CO) is prevalent in transition metal compounds with ions, which have a mixed valence, i.e. the average valence of an ion is not an integer. In CO-based multi-ferroicity, the arrangement of ions of different valences breaks spatial inversion symmetry and a polarization is induced. This is in addition to the existence of a spin degree of freedom on the mixed valence transition metal. The involvement of the same electrons or sites in charge and spin order can lead to strong magneto electric coupling **[Angst, 2013]**.

There are not many examples of materials in which multi-ferroicity is caused by CO. $LuFe_2O_4$ was one of these famous cases, as it was thought to be ferroelectric due to charge ordering **[Ikeda at al., 2005]**. However, in recent experiments, it was shown it is not the case, as discussed in the next section. Another example is Magnetite (Fe_3O_4), which is a complex charge-ordered crystal structure that was recently understood **[Senn et al., 2012]** and found to be polar. In addition, macroscopic measurements indicate a switchable polarization **[Schrettle et al., 2011].**

1.2 RFe_2O_4 Materials

An interesting example of transition metal oxides is the rare earth ferrites material class RFe_2O_4 with R being a 3+ ion (Y, Ho, Er, Tm, Yb, Lu, or In). It crystallizes in a rhombohedral structure (Figure 1.6), with alternate triangular lattices of $Fe_2O_{2.5}$ bilayers (labelled W in the figure) separated by $RO_{1.5}$ monolayers (U) **[Qin et al. 1, 2009]**.

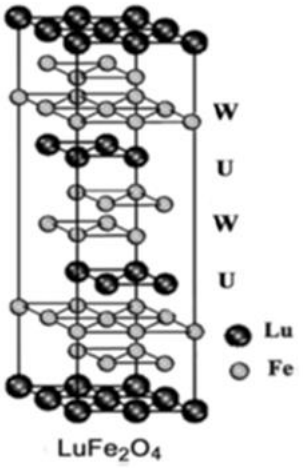

Figure 1.6 $LuFe_2O_4$ crystal structure. Taken from [Qin et al. 1, 2009].

In RFe_2O_4, the Fe ion has an average valance of 2.5+, implying an active charge degree of freedom, and the spin of iron is present also, therefore a coupling between these two degrees of freedom is likely. An equal amount of Fe^{2+} and Fe^{3+} coexists on the triangular lattice, so the interactions between the Fe^{2+} and Fe^{3+} show frustration in charge. Similarly, the ordering of the Fe magnetic moments is affected by the same geometrical frustration as the CO, shown in figure 1.1.

RFe_2O_4 attracted a lot of attention in particular due to the proposed new mechanism of ferroelectricity arising from charges ordering (CO), of Fe^{2+} and Fe^{3+} in the Fe/O bilayers **[Ikeda et al., 2005]**. Ikeda **[Ikeda et al., 2005]** proposed in 2005 that the Fe/O triangular bilayers of $LuFe_2O_4$ are charge ordered as shown in figure (1.7a), for which one of the layers is rich in Fe^{2+} and the other is rich in Fe^{3+}, which implies that the bilayer is polar, i.e. this CO would be ferroelectric.

$LuFe_2O_4$ was considered a clear example of ferroelectricity from CO, but in recent work by the host group **[de Groot et al. 1, 2012]**, the structural refinement of single crystal X-ray

diffraction data and bond-valence-sum (BVS) analysis showed a charge order in the bilayers different from what was proposed by Ikeda. This new CO indicates that $LuFe_2O_4$ is not ferroelectric at all and the charged bilayers are not polar (Figure 1.7b). The absence of polarity is confirmed by dielectric measurements and polarization hysteresis loops measured by [**Niermann et al., 2012], [Ruff et al., 2012] and** later by [**Lafuerza et al., 2013]**. However, although ferroelectricity from CO is disproved in $LuFe_2O_4$, it might in principle still be realized for other members of this family.

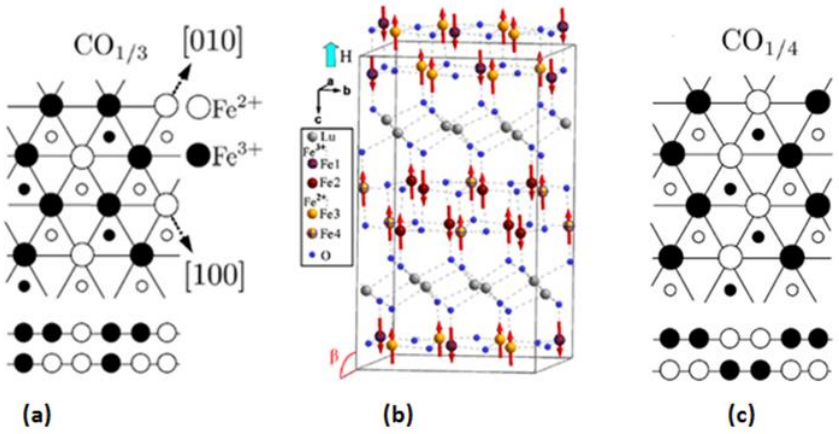

Figure 1.7 (a) Proposed ferroelectric charge configuration in Fe/O bilayer in RFe_2O_4 (Fe ions in upper/lower layer are drawn as large/small circles). Taken from [Naka et al., 2008]. (b) The experimentally established CO pattern of $LuFe_2O_4$. Taken from [de Groot et al. 1, 2012]. (c) An alternative CO that has been considered theoretically. Taken from [Naka et al., 2008].

Many other intriguing features contributing to the high interest have been noticed in different RFe_2O_4 such as e.g. oxygen storage capacity **[Hervieu et al., 2014]**, gas sensing **[Cao et al., 2012]**, exchange bias **[Sun et al., 2013]**, giant coercivity **[Wu et al., 2008]**, and magnetic phase competition due to geometric frustration **[de Groot et al. 2, 2012]**. All these phenomena are related to underlying charge and spin ordering processes, which despite of the intense recent research are still not sufficiently understood **[Angst, 2013].**

1.2.1 Interactions and their tuning by structural modification

The Coulomb repulsion between the excess electrons in Fe^{2+} is supposed to drive the charge ordering with Fe^{2+} and Fe^{3+} being arranged in order to minimize the electrostatic energy. In models, at least four (screened) coulomb interactions are necessary to explain the appearance of 3D charge ordering **[Yamada et al., 2000]** : an intralayer interaction U_1, the interlayer nearest neighbor interaction within the bilayer U_2, and the interaction between different bilayers U_3, U_4 (Figure 1.8). Similar considerations hold for the magnetic interac-

tions driving spin orders, where for 3D order to occur, an equivalent minimal set of interactions is necessary.

For a first analysis of the CO in one bilayer, it is sufficient to consider U_1 and U_2. Considering only U_1, the geometrical frustration on the triangular lattice leads to many degenerate charge order patterns (including all shown in figure 1.7).

Taking into account U_2, this degeneracy is broken : of the COs shown in figure 1.7, a repulsive U_2 makes the one of panel c most stable and the one of panel b least stable **[Angst, 2013]**. The fact that the CO of figure 1.7b is the one experimentally found for $LuFe_2O_4$ **[de Groot et al. 1, 2012]** suggests that contributions other than electrostatic ones are important in stabilizing the CO. This is also indicated by density-functional-theory (DFT) calculations on $LuFe_2O_4$, which indicate a significant impact of both magnetism **[Xiang et al., 2009]** and the lattice **[Xiang et al., 2007]** on the CO. The former is consistent with the strong spin-charge coupling found by XMCD **[de Groot et al. 1, 2012]**.

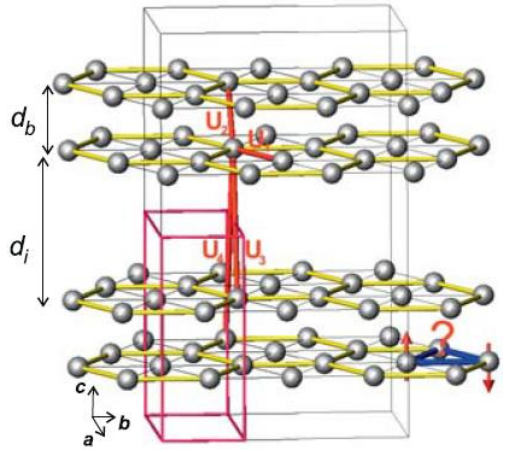

Figure 1.8 Minimum set of interactions U1…U4 leading to 3D charge ordering. Geometrical frustration is indicated by blue triangle. Taken from [Angst, 2013].

The lattice contribution to the stability of different charge ordering patterns is clear, where the lattice relaxation would further lower the energy of CO phases. It is clear that the lattice relaxation is very important as the experimental structure is very heavily distorted. In $LuFe_2O_4$, density functional theory calculations showed that the ferroelectric CO (Figure 1.7a) and a stripe-like CO with $(\frac{1}{2}\ \frac{1}{2})$ in-plane propagation (Figure 1.9) were stable in the absence of geometric relaxation, whereas after structural relaxation, the ferroelectric CO remained only slightly more stable than the strip-like CO structure **[Xiang et al., 2007]**.

The magnetic contribution, which is likely, is also very important, in the light of the strong spin-charge-coupling experimentally observed in $LuFe_2O_4$ by different techniques. **[Angst et al., 2008].** It was found that the incommensurability of the CO has a minimum at the Neel temperature, and the Mossbauer spectroscopy measurements of **[Nakamura et al., 1998]** revealed that all Fe^{2+} spins and one third of the Fe^{3+} spins are aligned parallel to magnetic field whereas the remaining Fe^{3+} are aligned antiparallel **[Angst, 2013].** This was confirmed later by XCMD studies **[de Groot et al. 1, 2012] and [Ko et al., 2009].**

Xiang suggests that the energy-differences between various magnetically ordered states are of the same order as the energy gain by lattice relaxation **[Xiang et al., 2009]**. Despite these additional factors, a controlled tuning of U_1 and U_2 can be expected to stabilize different COs in a systematic way.

For example, increasing U_2 (relative to U_1) should make the CO of figure 1.7c more likely. According to figure 1.8, this can be achieved by increasing the rare earth ion size (decreasing the bilayer thickness d_b will increase U_2 based on coulomb law). The ion size effect may systematically tune the magnetic and lattice contributions to the CO stability.

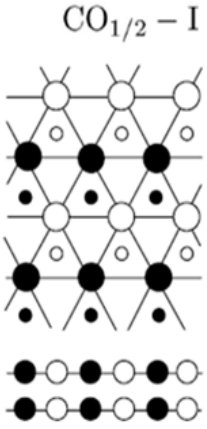

Figure 1.9 A stripe-like CO with (1/2 1/2) in-plane propagation vector (Fe ions in upper/lower layer are drawn as large/small circles). Taken from [Naka et al., 2008].

The ion size of Yb^{3+} is almost the same as that of Lu^{3+} (Figure 1.10), hence the same CO is expected for both, which was confirmed by recent X-ray and neutron diffraction results **[Williamson et al., unpublished]**. In contrast, Y^{3+} is much larger, and a different CO was

found **[Mueller et al., 2015]**, where YFe_2O_4 showed superstructure reflections described by a propagation vector (1/4 1/4 3/4) at 160 K.

An in-plane four times enlarged superstructure was previously observed in micro-crystals by electron diffraction by **[Horibe et al., 2004]** at 150 K. Such fourfold CO as shown in Figure (1.7c) was found theoretically to be the ground state for certain interaction strengths **[Naka et al., 2008]**. However, a less favorable electrostatically CO was refined by Mueller **[Mueller et al., unpublished]**, and demonstrated, as in $LuFe_2O_4$, the importance of additional lattice and magnetic contributions.

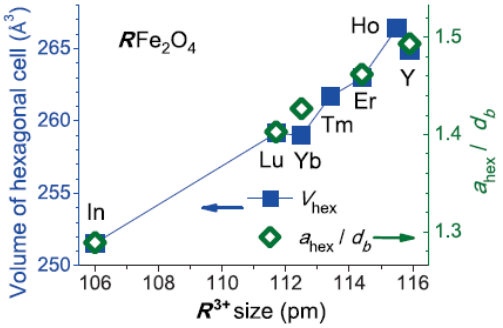

Figure 1.10 R^{3+} ion size effect on cell volume and ratio of intralayer Fe–Fe distance a_{hex} to bilayer thickness d_b. Taken from [Angst, 2013].

Given the completely different CO in $LuFe_2O_4$, and YFe_2O_4, it is of high interest to elucidate the evolution of charge and spin order as a function of rare earth size by a partial substitution, e.g. $Lu_xY_{1-x}Fe_2O_4$.

1.2.2 Impact of the oxygen stoichiometry

One critical aspect of this study is the need to fine-tune the oxygen-stoichiometry, as otherwise, it is impossible to distinguish oxygen stoichiometry changes from the effect of rare earth substitution. The synthesis therefore has to be done under a tunable flow of CO and CO_2 to control the oxygen partial pressure.

It has been observed experimentally that the oxygen-stoichiometry leads to a strong variation in physical properties; where for example in YFe_2O_4 oxygen-stoichiometry affects both magnetization and CO **[Mueller et al., 2015]** and **[Inazumi et al., 1981]**. The off-stoichiometric samples exhibit a broad peak in zero-field cooled (ZFC), M(T) indicating a glassy magnetic state. In contrast, the stoichiometric case exhibits two well-defined transitions to an antiferromagnetic state as shown in figure 1.11. Meanwhile, YFe_2O_4 is available

with oxygen stoichiometry variations from $YFe_2O_{3.905}$ to $YFe_2O_{4.000}$ according to the Fe-Fe_2O_3-Y_2O_3 phase diagram established by **[Kimizuka and Katsura 1, 1975]**. Another group found a slightly higher lower stability limit $YFe_2O_{3.9115}$ **[Jacop and Rajitha, 2012]**.

The influence of the oxygen-stoichiometry on the magnetization is observed for both $LuFe_2O_4$ and $YbFe_2O_4$ as well. **[Sekine and Katsura, 1976]** found that $LuFe_2O_4$ has oxygen stoichiometry variations from $LuFe_2O_{3.937}$ to $LuFe_2O_{4.015}$, while for $YbFe_2O_4$ it varies from $YbFe_2O_{3.929}$ and $YbFe_2O_{4.052}$ **[Kimizuka and Katsura 2, 1975]**.

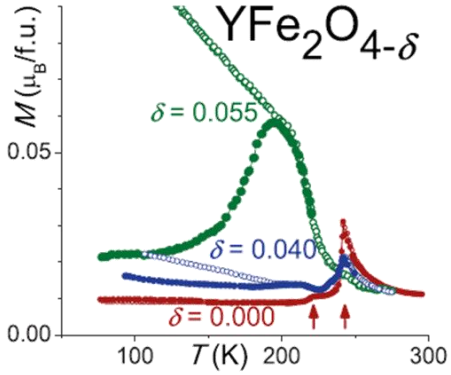

Figure 1.11 Magnetization measurements of different stoichiometry $YFe_2O_{4-\delta}$ represent the oxygen deficiency. Taken from [Angst, 2013].

Figure 1.12 shows the magnetization measurements of single crystalline $LuFe_2O_4$ grown by Angst under different CO_2:CO gas mixtures conducted by **[de Groot, 2012]**. A classification of the magnetic behavior was done for crystals with different oxygen stoichiometry. The crystal classified as type A exhibit the best stoichiometry in which the field cooled (FC) curve shows a very sharp peak transition at 238 K while the type B samples shows an average stoichiometric quality, in this sample the transition peak magnetization was slightly decreased and the transition was shifted as well to 230 K.

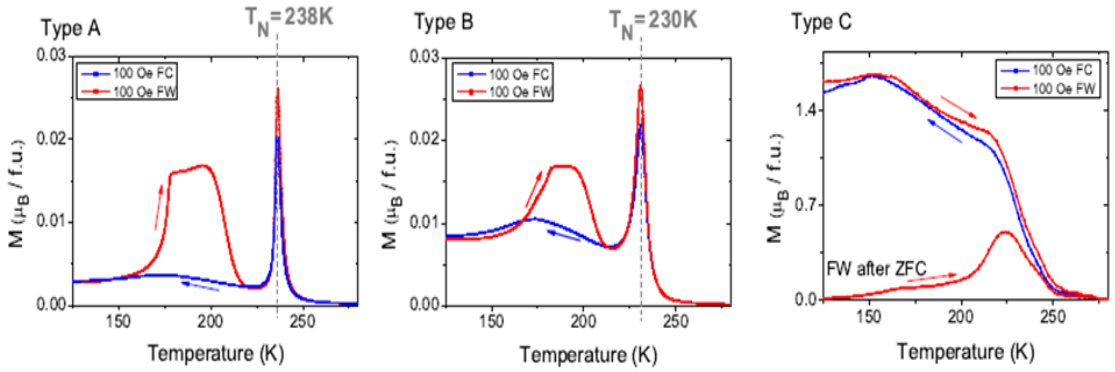

Figure 1.12 Magnetization measurements of different stoichiometry $LuFe_2O_4$ [de Groot, 2012].

Type C was classified as a poor stoichiometry crystal compared to A and B in which a very different behavior was observed. The FC curve shows a broad peak indicating a glassy magnetic behavior. Therefore, e.g. magnetization measurements are necessary to check the stoichiometry.

1.2.3 The study of $Lu_xY_{1-x}Fe_2O_4$ compound

Kishi classified polycrystalline $Lu_xY_{1-x}Fe_2O_{4-\delta}$ (x=0.02, 0.05, 0.1, 0.2, and 0.5) **[Kishi et al., 1983]**. According to their T-dependent magnetization in a relatively high field (Figure 1.13): for x=0.02, 0.05, and 0.1 the magnetic behavior is distinct from both YFe_2O_4 and $LuFe_2O_4$. Therefore, we expect a new charge and spin order. For x=0.2 and 0.5 the magnetic behavior corresponds to (slightly off-stoichiometric) $LuFe_2O_4$, hence we expect a CO identical (or very similar) to $LuFe_2O_4$ **[de Groot et al. 1, 2012] and [Wang et al., 2013],** provided that the sample is stoichiometric enough.

Serrao investigated the low-field magnetization of $Lu_{0.5}Y_{0.5}Fe_2O_4$, though without addressing the stoichiometry and observed the occurrence of ferrimagnetism around 250 K **[Serrao et al., 2008]**. Moreover**,** Yoshii investigated the magnetization of $Lu_{0.5}Y_{0.5}Fe_2O_4$ without addressing the stoichiometry as well but under a higher magnetic field **[Yoshii et al., 2008]**. Finally, Noh investigated polycrystalline $Lu_xY_{1-x}Fe_2O_4$ by X-ray magnetic circular dichroism, which is less sensitive to oxygen stoichiometry **[Noh et al., 2010]**.

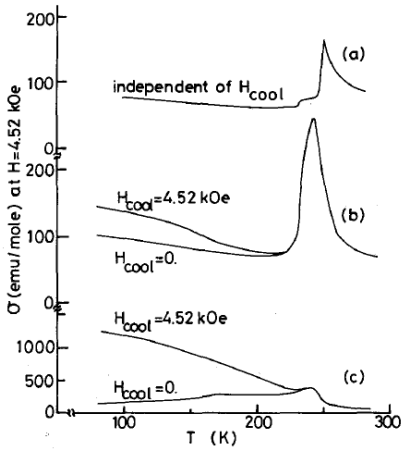

Figure 1.13 Magnetization behavior of polycrystalline $Lu_xY_{1-x}Fe_2O_{4-\delta}$. Taken from [Kishi et al., 1983].

1.3 Place and Profile of Research

1.3.1 Research Place

The experimental work of this thesis was conducted at the Forschungszentrum Jülich in Germany, at the Jülich Centre for Neutron Science (JCNS-2) (see figure 1.14).

The JCNS, which is part of the institute for solid-state research (IFF), Forschungszentrum Jülich GmbH, was founded in 2006 to operate a state-of-the-art neutron scattering instruments using the most modern and highest flux neutron sources in the world. JCNS develops and operates neutron scattering instruments at some of the best neutron sources worldwide. In-house research focuses on correlated electron systems, Nano magnetism, soft matter and biophysics. JCNS consists of two institutes: JCNS-1 investigates the structure and dynamics of soft matter using neutron scattering, develops neutron scattering instruments and makes them available to external researches through the JCNS, while JCNS-2 develops and uses scattering techniques to understand the structural and magnetic order, fluctuations and excitations in magnetic systems and in highly correlated electron systems at the atomic level. JCNS operates their instruments at the FRM 11 reactor at the MLZ in Garching, Germany, the SNS Spallation Source in Oka Ridge, USA, and the ILL high-flux reactor in Grenoble, France" **[JCNS brochure, 2009]**.

Figure 1.14 Jülich Centre for Neutron Science institute (JCNS-2)

1.3.2 Research Profile

The aim of this thesis is to study "how charge and spin orders change while tuning the relevant interactions by gradually increasing the rare earth ion radius, made by substitution", i.e. the substitution of Y in $LuFe_2O_4$. The strength of U_1 is expected to get weaker relative to U_2 by increasing the in-plane lattice constant since the ionic size of Y is larger than that of Lu (Figure 1.8).

In order to achieve this aim, polycrystalline samples were synthesized under a controlled oxygen partial pressure **[Shindo et al., 1976]** using CO_2-H_2 (4%)/Ar (96%) at 1250 ˚C to fine tune the oxygen-stoichiometry. $Lu_{0.5}Y_{0.5}Fe_2O_{4-\delta}$ was synthesized to verify that this composition, though halfway towards Y, behaves like pure $LuFe_2O_4$ **[Kishi et al., 1983].** Then the samples with a higher percentage of Y i.e. $Lu_{0.1}Y_{0.9}Fe_2O_{4-\delta}$ was prepared to test their rather odd magnetic behavior, which is distinct from both $LuFe_2O_4$ and YFe_2O_4 **[Kishi et al., 1983]**. Characterizations by X-ray powder diffraction to check the phase purity, and low-field magnetization to indicate the stoichiometry have been done. The characterization results were used as a feedback to optimize the synthesis parameters.

To investigate the CO and spin order in the prepared samples, diffraction is necessary, but based on experience **[Angst, private communication],** the associated reflections are too weak to be resolved in polycrystalline samples. Therefore, single crystal samples are neces-

sary. The optical floating zone (OFZ) method with a CO-CO_2 atmosphere was used for crystal growth because controlling the oxygen partial pressure during growth is essential to obtain stoichiometric single crystals. As for polycrystalline samples, feedback from X-ray diffraction and magnetization measurements of the single crystals was used to optimize the quality (in particular the oxygen stoichiometry) of the crystals. The CO was investigated in-house with the same single-crystal X-ray diffractometer that was already used to determine the CO of $LuFe_2O_4$ **[de Groot et al. 1, 2012].** Neutron diffraction is necessary to determine the spin order, but this remains for future work.

2 *Experimental Methods*

In this chapter a review of the various experimental techniques used in the work is made. The first section deals with sample preparation methods, whereas the second one introduces the utilized characterization techniques.

2.1 Sample Preparation

Both polycrystalline powders and single crystals were prepared during the course of this work. Polycrystalline samples of $Lu_xY_{1-x}Fe_2O_{4-\delta}$ with x=0.5 and 0.1 were prepared by a solid state reaction in a mixed flow of CO_2 and Ar-H_2 **[Shindo et al., 1976]**. To achieve the aim of the investigating the CO and (spin order, later on) of $Lu_xY_{1-x}Fe_2O_{4-\delta}$ as discussed in the introduction, the fabrication of single crystals is essential. The floating zone method (FZ) was used to grow the required single crystals.

2.1.1 Powder synthesis

Polycrystalline samples of $Lu_xY_{1-x}Fe_2O_{4-\delta}$ were synthesized based on solid state reactions from stoichiometric (with respect to the metal ions) mixtures of high purity Y_2O_3, Lu_2O_3 and Fe_2O_3. The used stoichiometric mixing molar ratio in $Lu_{0.5}Y_{0.5}Fe_2O_{4-\delta}$ is 0.25:0.25:1 sequentially and 0.45:0.05:1 in $Lu_{0.1}Y_{0.9}Fe_2O_{4-\delta}$. After mixing and ballmilling under isopropanol to get a very fine powder (isopropanol is used to facilitate a better mixing), the raw material was dried in a nitrogen atmosphere at 70° C and then filled into a Al_2O_3 boat. Afterwards, the powder was calcinated in a tube furnace under controlled oxygen partial pressure using CO_2-H_2(4%) at 1250 $^\circ$C, for roughly 8 hours. The time-temperature sintering profile is shown in figure 2.1.

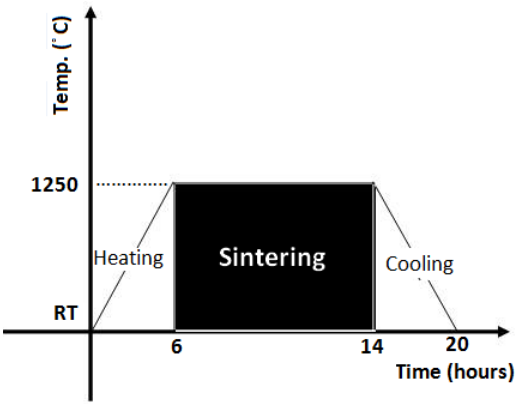

Figure 2.1 Time-temperature profile used for both calcination and sintering.

Tuning the CO_2-H_2(4%) ratio of the gas flow, gives us the ability to control the oxygen partial pressure in the surrounding atmosphere, which is critical to form the divalent and trivalent iron in RFe_2O_4 **[Shindo et al., 1976],** the change of valences in exchange with the surrounding oxygen is based on the following reaction :

$$2\ Fe^{2+} + ½\ O_2 = 2\ Fe^{3+} + O^{2-} \qquad 2.1$$

A specific ratio of CO_2-H_2(4%) at a constant temperature, leads to a series of equilibrium reactions creating free oxygen at a very low partial pressure **[Shindo et al., 1976]**:

$$CO_2 = CO + ½\ O_2 \qquad 2.2$$

$$CO_2 + H_2 = H_2O + CO$$

$$H_2O = H_2 + ½\ O_2$$

The resulting oxygen partial pressure determines phase stability and oxygen stoichiometry **[Sekine and Katsura, 1976].** Finally, the sintered powder is ball milled and dried in a nitrogen atmosphere again. The subsequent preparation steps are sketched in figure 2.2.

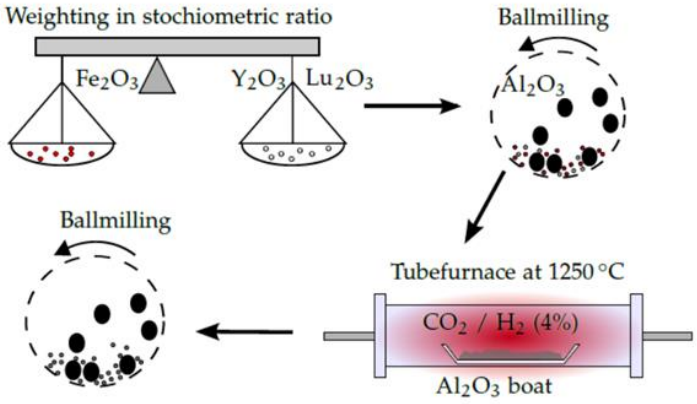

Figure 2.2 Systematic view of the powder synthesis. Taken from [Mueller, 2012].

Each powder calcinated at specific CO_2-H_2(4%) gas flow is characterized by XRD described later in section (2.2.1.1) to check the phase purity and by low-field magnetization measurements (Section 2.2.2) examine the stoichiometry.

2.1.2 Single crystal growth

The Optical Floating Zone (OFZ) method is used for the crystal growth based on the possibility to control the atmosphere and the avoidance of contamination since no crucible is present. In order to obtain a high quality crystal, the oxygen partial pressure is controlled by applying the gas flows of CO_2 and CO during the growth. CO_2/CO is used instead of CO_2/H_2 (4%) to avoid the formation of water, which would result in disturbance of the crystal growth **[Iida et al., 1990].** Actually, this method was used successfully to prepare high-quality crystals of $LuFe_2O_4$ **[Christianson et al., 2008]**, and YFe_2O_4 **[Mueller et al., 2015]**.

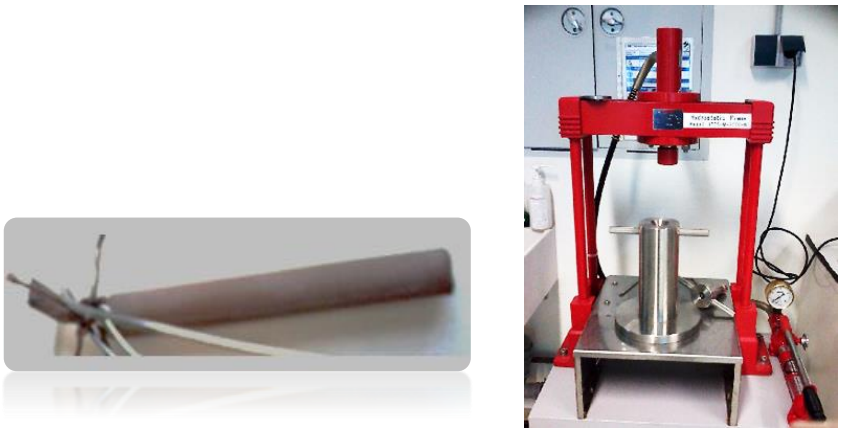

Figure 2.3 Left side: The evacuated sealed polycrystalline rod before compression. Right side: The used HPTS-M-2000-W hydrostatic press.

To start a crystal growth a polycrystalline rod is necessary. Therefore, the prepared polycrystalline material (section 2.1.1) is filled into a latex tube homogenously, which is then evacuated and well-sealed (see left side of figure 2.3). Afterwards, the tube is pressed hydrostatically under a pressure of 30 MPa for roughly an hour. Distilled water is used inside the hydrostatic compression (right side of figure 2.3) to collect the powder, if the tube is destroyed. After compression, the latex tube is removed, and the 6-8 cm long formed rod is sintered utilizing the same tube furnace used for the powder synthesis with the same time-temperature profile showed in figure 2.1. Finally, a dense straight uniform rod is obtained.

The apparatus used for crystal growth is a four-mirror furnace FZ-T-10000-H-VI-VP0 shown in figure 2.4 (left side). The growth chamber shown in figure 2.4 (right side) consists

of four elliptical mirrors, which focus the light from the halogen lamps placed at the foci of the mirrors creating a localized hot zone. Two polycrystalline rods are used for crystal growth : a 6-8 cm feed rod and 1-2 cm seed rod, both rods are aligned vertically at the center of rotation of the upper and lower shafts. The feed rod hangs freely hold by a platinum wire from the upper shaft at the top of seed rod, which is fixed to the lower shaft using a ceramic tube. The upper and lower shafts are rotating in opposite directions for a homogenous heat distribution and mixing of the material in the molten zone. A quartz tube is used to isolate the crystal growth region from the ambient atmosphere, this enables to offer the desired gas atmosphere during the growth.

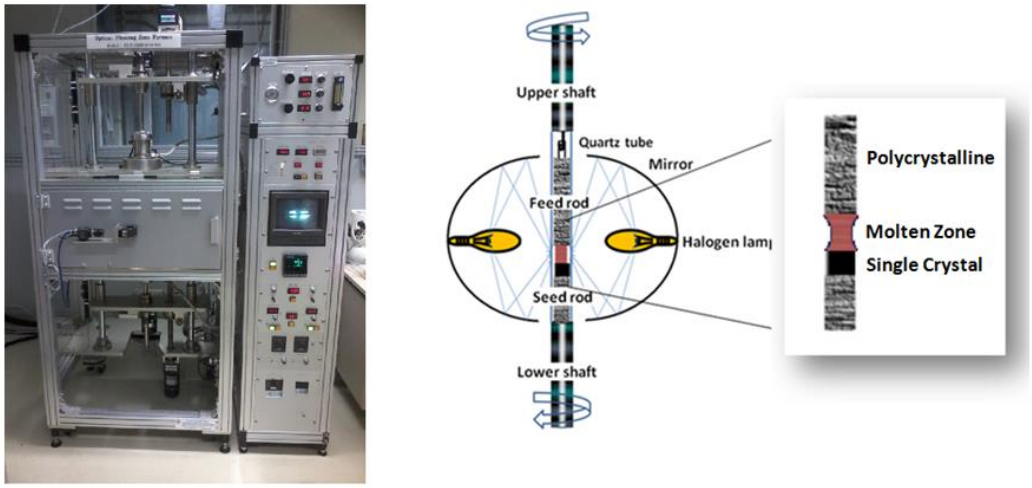

Figure 2.4 Left side : Four-mirror furnace FZ-T-10000-H-VI-VP0 used in crystal growth. Right side: Sketch crystal growth chamber setup.

After mounting the feed and seed rods vertically with a few mm separation between both the quartz tube, the sample chamber was flushed with Ar to remove atmospheric oxygen, afterwards the heating process starts and CO_2 /CO gas continuously flows into the growth region. The growth process starts with melting the tips of the seed and feed rods by bringing them into the hot zone and, then connecting them, thereby producing a molten zone. This molten material is kept from dropping down by the surface tension. The upper and lower shafts are then both slowly moved downwards. This causes more and more of the feed rod to melt, while crystals on top of the seed rod grow. We have chosen a growth speed of 1 mm/hour since growth speeds below 2 mm/h have been found essential to grown YFe_2O_4 **[Shindo et al., 1976]**. The melt settled on the top of the seed forming crystallites.

2.2 Characterization methods

Scattering experiments were performed to obtain a detailed insight on a microscopic level, including X-ray powder diffraction for confirming phase purity, Laue diffraction for orientation of the crystal and single crystal X-ray diffraction for in-depth investigation of the CO. Moreover, sophisticated characterization methods were used to check the quality of the samples, where feedback megneto-metry and thermogarvimetry is used to optimize the quality of the sample (in particular oxygen stoichiometry) by tuning the synthesis parameters of both powders and crystals.

2.2.1 Scattering techniques

Scattering is a gentle method used to investigate the structure of material and to explain its macroscopic properties. In the scattering experiment, a monochromatic beam described by a plane wave with wave vector $\underline{k}$ ($|\underline{k}| = 2\pi/\lambda$) hits the target producing a scattered wave described by a wave vector $\acute{\underline{k}} = \underline{k} + \underline{Q}$ as shown in figure 2.5.

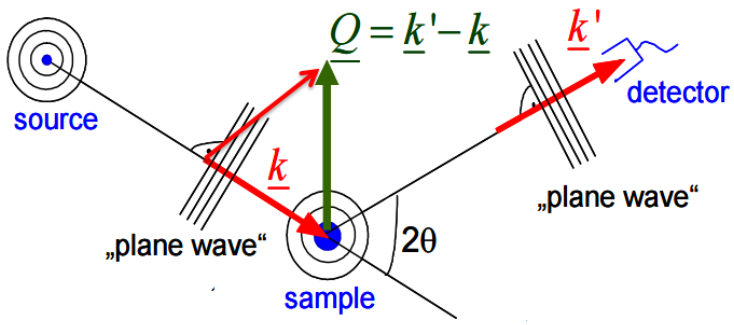

Figure 2.5 Sketch of scattering process. Taken from [Neutron lab course book, 2013].

Diffraction is elastic coherent scattering **[Neutron lab course book, 2013]** in which the energy is conserved during the scattering process. So $|k| = |\acute{k}| = 2\pi/\lambda$ and the scattering vector $\underline{Q} = \underline{\acute{k}} - \underline{k}$.

For atoms arranged periodically interference effects lead to Bragg diffraction, as shown in figure 2.6. If the separation distance between atoms is comparable to the wavelength (λ) of the X-rays. The X- rays incident parallel to each other making an angle θ with the plane of atoms, each plane reflects only a small fraction of the incident wave. The X-rays will interfere constructively when the path length difference ($2\ d\ \sin\theta$) is equal to an integer multiple of the wavelength λ summarized in Bragg's law :

$$2\,d\sin\theta = n\,\lambda, \qquad 2.3$$

where d is the spacing between parallel atomic planes.

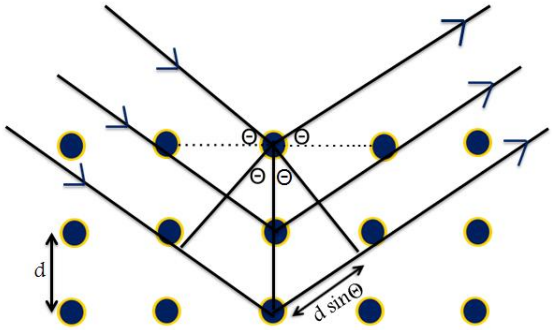

Figure 2.6 Illustration of Bragg's law where a constructive interference occurs only when the path length difference is equal to a multiple integer of λ.

2.2.1.1 Powder X-ray diffraction

Powder diffraction is a non-destructive tool to confirm the formation of the desired compound and to check the phase purity.

In a powder diffraction experiment, a monochromatic X-ray beam shines on a sample consisting of many tiny randomly oriented crystals and it is scattered by the electrons of the atom. A detector scans around horizontally to collect the directions and intensities of the outgoing diffracted waves. A 1-D diffraction pattern emerges with peaks of the intensity occurring for all scattering angles 2θ that satisfy the Bragg condition.

A few milligrams of very-fine powder are distributed homogenously over the sample holder by using a few drops of isopropanol, and then the holder is mounted in the X-ray diffractometer. The powder X-ray diffraction is performed at RT in a transmission geometry. The diffraction is done by using Cu-K_α radiation with wavelength 1.54 Å and the data is collected by a Huber G670 Gunier-camera. A diffraction pattern representing the intensities corresponding to different spacing between the lattice planes is produced. See figure 2.7.

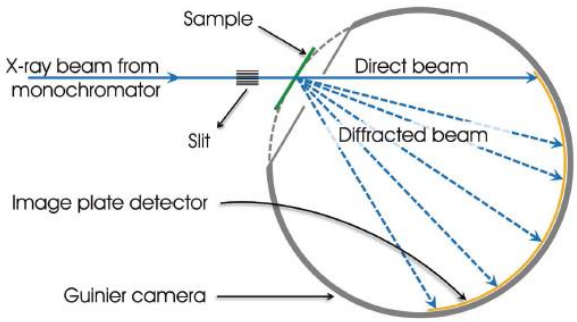

Figure 2.7 Transmission geometry powder diffraction. Taken from [Kumar, 2012].

To identify the formed compound, the peak positions and intensities of the collected diffraction patterns are compared with standard diffraction patterns obtained by simulation of the diffracto-gram of a structure averaged from the structures of $LuFe_2O_4$ and YFe_2O_4 as found in the International Crystallographic Database (ICSD). In case that additional peaks cannot be indexed with the target phase, their positions and intensities are compared with potential impurity phases. The foreign phases in the diffraction patterns of different stoichiometric samples are identified by comparing with the (ICSD) published data **[ICSD website]**. The presence and composition of foreign phases were used to optimize the synthesis conditions as will be shown in a later section.

Powder XRD data may be used to refine lattice parameters and even crystal structures, but in my work, the main purpose was to check the phase purity.

2.2.1.2 Laue diffraction

This technique is used for determining the orientations of single crystals of a known structure for various microscopic or macroscopic measurements, (in our case magnetization measurements), and find if crystal is really a single grain. This type of diffraction is different from powder and single-crystal diffraction since Laue diffraction uses a polychromatic "White" ray beam comprising a range of wavelengths.

Since the crystal is irradiated with of a wide interval of wavelengths, the Bragg condition will always be fulfilled for some lattice planes regardless of the orientation of the crystal, and backscattered on the area detector. The Orient Express software is used to simulate the formed Laue pattern. Then the crystal is rotated according to this image until we obtain the

desirable orientation. For a sample orientation with a high-symmetry axis parallel to the incoming beam, that symmetry is visible in the diffraction pattern.

2.2.1.3 Single crystal X-ray diffraction

Single crystal X-ray diffraction is performed to investigate the charge order of the samples. Because the sample is a single crystal and a monochromatic beam is used, the Bragg condition is fulfilled only for specific orientations of the sample. An experiment consists of stepwise rotations of the crystal, with the diffraction pattern for each step being collected by an area detector. The instrument software then allows determining the unit cell of the crystal. The single crystal X-ray diffraction experiment is performed on a dual wavelength micro-focus diffractometer (Supernova), see figure 2.8.

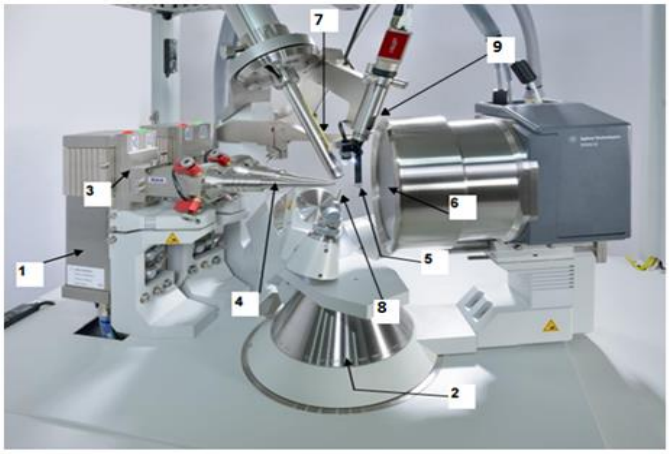

1. X-ray tube (front Cu K_α, back Mo K_α)
2. 4-circle Kappa goniometer
3. X-ray Shutter
4. Collimator
5. Beamstop
6. (Beryllium Window) CCD detector
7. Cryoject
8. Sample holder
9. Camera for sample alignment

Figure 2.8 Supernova diffractometer. Taken from [Supernova User Manual, 2014].

Two X-ray sources provide different wavelengths: molybdenum (Mo) with λ= 0.709 ˚A or copper (Cu) with λ=1.540 ˚A. The Molybdenum X-source is used in our diffraction experiments to access a larger portion of the reciprocal space (more reflections) and to avoid stronger absorption and strong Fe-K_α florescence. This is the case because the Fe K-absorption edge is at 7.1 keV and the corresponding K_α florescence line is at 6.4 keV and Cu K_α energy is 8 keV, slightly higher than the Fe K-edge. A 4-axis Kappa goniometer

(omega, kappa, phi and theta axis) is used for sample orientation and a large area Charged Coupled Device (CCD) atlas detector to collect the diffracted rays **[Supernova User Manual, 2014]**.

The sample temperature is changed by Nitrogen gas flow in the range from 100 K up to 490 K. The CrysAlisPro software is used for collection, reduction and analysis of the data. Before starting a long experiment, a short pre-experiment is done to assess crystal quality (single grain or several grains) and determine the experiment strategy (what orientations will be scanned). Afterward a longer (several hours up to several days) experiment is started under different temperatures and a map of reciprocal hkℓ reflections is produced. Subsequently, one can integrate intensities of the reflections and do structure refinement.

For each growth, the produced crystals were checked by X-ray powder diffraction and by magnetization measurements to examine the stoichiometry.

2.2.2 Magnetization

Magnetization measurements are performed on the $Y_xLu_{1-x}Fe_2O_4$ by using a Vibrating Sample Magnetometer (VSM) option of both **the physical properties measurement system (PPMS)** and the **PPMS DynaCool** to check the stoichiometry of the samples.

We used the PPMS with the VSM option as a sensitive DC magnetometer in the measurement of the equilibrium values of the samples magnetizations under an applied magnetic field as a function of temperature in the range of 10-350 K. As well the field dependent magnetization was measured. In the PPMS used, the applied magnetic field can reach 9T, and the temperatures down to 4.2 K can be reached. The magnetization can be measured with a sensitivity of 10^{-6} emu.

The VSM option primarily consists of a linear motor for vibrating the sample with 40 Hz, and some pickup coils around the sample in the sample chamber. The basic measurement is accomplished according to Faraday's law of induction. The sample is attached to the end of a sample rod, and vibrates between a set of pickup coils. Therefore the position of the magnetic moment of the sample (which is magnetized by a static magnetic field) about the pickup coils changes. This changes the magnetic flux in the pickup coils, therefore voltages

are induced in the pickup coils, from which the magnetic moment of the sample can be deduced. See figure 2.9.

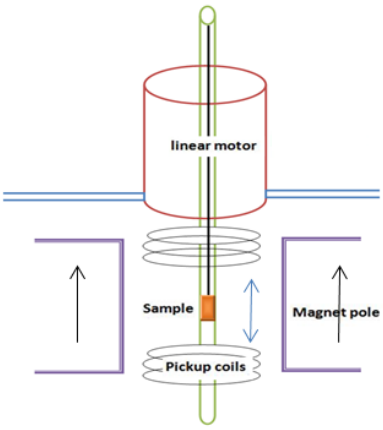

Figure 2.9 VSM option of the PPMS setup.

Low-field magnetization measurements were done on both powder and single crystals in the temperature range of 10-300 K with an applied magnetic field of 100 Oe and a sweep rate of 2 K/min to indicate the stoichiometry and thus optimize the synthesis parameters.

The change of the magnetization as a function of the temperature was examined with three modes: the Zero field Cooling (ZFC) mode in which the system is cooled in zero magnetic field before the measurement, which is done in a field during warming; the Field Cooling (FC) mode in which the magnetization is measured during cooling in a field; and the Field Warming (FW) mode in which the magnetization is measured in an applied field while increasing the temperature.

The PPMS DynaCool is the next generation Physical Property Measurement System (PPMS), and works using the same principle as PPMS but does not need an external supply of liquid cryogens **[Dynacool user's manual].** It provides a temperature range of 1.4-400 K and a magnetic field of 9 T field as PPMS.

2.2.3 Thermo-Gravimetric-Analysis (TGA)

The oxygen content of polycrystalline $Lu_{0.5}Y_{0.5}Fe_2O_{4-\delta}$ samples exhibiting different magnetic behaviors was studied using thermogravimetric analysis.

TGA is a thermal method used to determine the oxygen content by measuring the mass difference as a function of temperature. The sample of known mass is heated and/or cooled in

either a reducing or oxidizing (not used here) gas environment to induce a reaction to compounds of known oxygen stoichiometry.

The basic instrumental component for TGA is a thermo balance which is a microbalance with 1μg sensitivity placed in a furnace controlled by a temperature programmer with a linear rate. These components are enclosed by a container to allow a controlled flow of a specific gas (see figure 2.10). The result is a curve representing a mass change as a function of both temperature and time.

A few grams of the sample were put in a sample pan (Al_2O_3 crucible) which is supported by a high-precision balance under a reducing atmosphere in a closed furnace. Afterward the sample was heated in a reducing atmosphere CO_2:H_2(4%), in which the $Lu_{0.5}Y_{0.5}Fe_2O_{4-\delta}$ decomposes into Lu_2O_3, Y_2O_3, Fe and O_2. Because the gaseous O_2 disappears from the crucible, the reaction

$$4Y_{0.5}Lu_{0.5}Fe_2O_{4-\delta} \longrightarrow Lu_2O_3+Y_2O_3+8Fe+ (5-2\delta)O_2 \qquad 2.4$$

Can be used to calculate the oxygen off-stoichiometry δ from the weight change. There are many error sources affecting the experimental result, such as the error produced by using a microbalance with 1 μg sensitivity, which will produce an error of 0.001 in δ. In addition to this, there exist systematic errors due to water adsorption by the sample. For the needed accuracy in δ, TGA is at the limit of what is feasible.

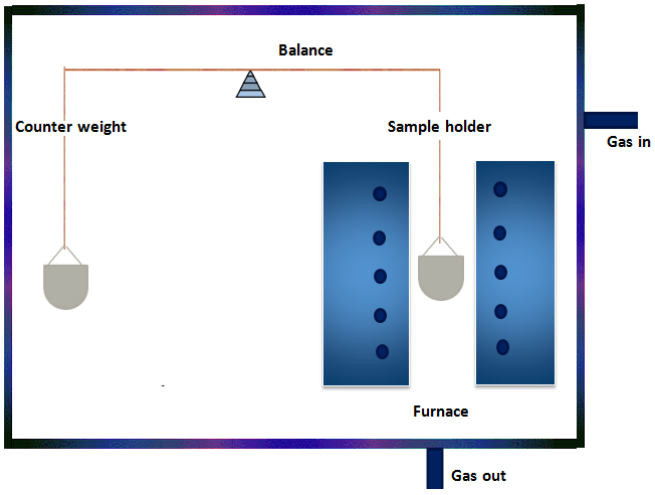

Figure 2.10 TGA instruments setup.

3

Results and Discussion

This chapter describes results obtained for both polycrystalline $Lu_{0.5}Y_{0.5}Fe_2O_{4-\delta}$ and $Lu_{0.1}Y_{0.9}Fe_2O_{4-\delta}$ and the present single crystal samples of $Lu_{0.5}Y_{0.5}Fe_2O_{4-\delta}$. For $Lu_{0.5}Y_{0.5}Fe_2O_{4-\delta}$, first of all, the prepared samples are shown. Afterward the selected characterization results are presented, addressed and discussed including the phase purity, low-field magnetization, the phase diagram, thermogarvimetry, and finally the CO. Whereas for $Lu_{0.1}Y_{0.9}Fe_2O_{4-\delta}$ only the phase purity and the magnetic behavior are addressed, within the time frame of the practical part of this thesis.

3.1 Polycrystalline $Lu_{0.5}Y_{0.5}Fe_2O_{4-\delta}$

Powder samples of $Lu_{0.5}Y_{0.5}Fe_2O_{4-\delta}$ were prepared under gas flows of different CO_2-H_2(4%) mixtures to control the oxygen-stoichiometry as described in section 2.1.1. These samples are summarized in Table 3.1 with the used gas ratio.

Name	CO_2 (ml/min)	Ar-H_2(4%) (ml/min)	CO_2/H_2
S1	5	30	4.17
S2	7	30	5.83
S3	8	30	6.67
S4	9	30	7.50
S5	11	30	9.17
S6	12	30	10.0
S7	13	30	10.83
S8	14	30	11.67
S9	15	30	12.5
S10	18	30	15

Table 3.1 Different polycrystalline $Lu_{0.5}Y_{0.5}Fe_2O_{4-\delta}$ samples calcinated under different gas ratios.

3.1.1 Phase purity

All samples were checked by powder X-ray diffraction at room temperature to verify the presence of a single phase.

The traditional method to check the phase purity is to compare the diffraction pattern of the compound with the data in the ICSD, but since no data for $Lu_xY_{1-x}Fe_2O_4$ is published, we averaged the peak position and intensity of YFe_2O_4 and $LuFe_2O_4$ from ICSD. In fact this is a relative intensities, but at least the peak position is good enough according to Vegard's law **[Vegard, 1921]** and thus fits well to our powder diffractogram.

Figure 3.1 shows the comparison between the standard diffractogram produced from calculation from ICSD i.e. reference and the diffractogram of the polycrystalline sample S1 prepared under the low gas ratio (5:30) which was collected in one hour.

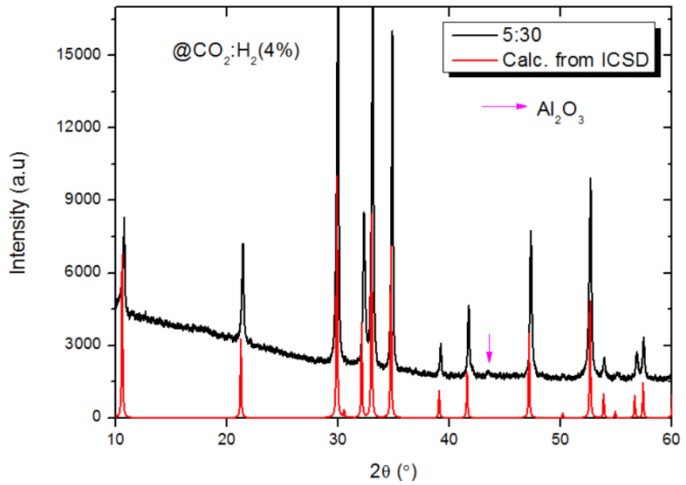

Figure 3.1 Comparison between powder XRD of S1 and the standard ICSD.

S1 matches very well with the standard one as no foreign peaks appear except for one peak at 43.5° (indicated by arrow in figure 3.1) identified as belonging to Al_2O_3 which is likely from the Al_2O_3 crucible used in the Ballmilling process.

All other samples were checked by X-ray diffraction as well, some of them are shown in figure 3.2. The peak at 43.5° is present in diffraction patterns of the all samples.

According to figure 3.2, $Lu_{0.5}Y_{0.5}Fe_2O_{4-\delta}$ is found as a pure stable phase in a wide region with gas ratios varying between 4.17 and 10.83. But for sample S10 which was prepared under the highest oxygen pressure (gas ratio 18:30), additional peaks appear, identified as due to an impurity of perovskite ($Lu_{0.5}Y_{0.5}FeO_3$) and FeO.

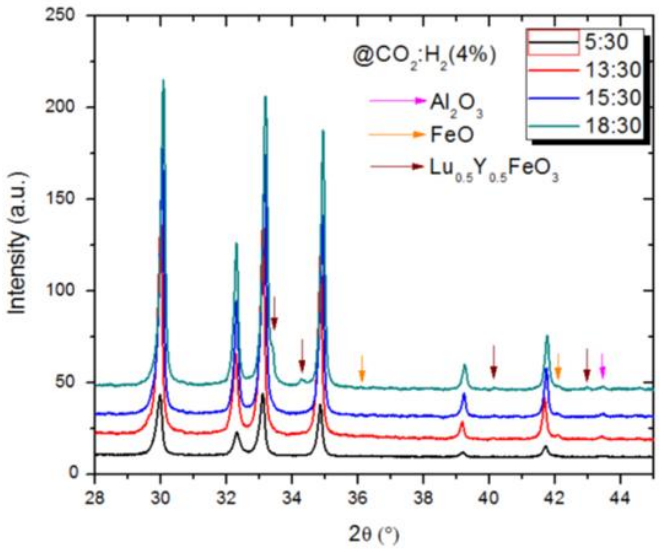

Figure 3.2 Powder XRD for different samples prepared under different gas ratios.

Both the perovskite $RFeO_3$ and wüstite are predicted phases for oxygen excess according to the YFe_2O_4 phase diagram shown in figure 3.3 and the most frequently observed foreign phases in YFe_2O_4 prepared under a too high gas ratio **[Shindo et al., 1976]** and **[Mueller, 2012].** Magnetite (Fe_3O_4) could be one of the expected foreign phases according to $LuFe_2O_4$ phase diagram **[Sekine and Katsura, 1976]**, but it has not been observed. Fe_2O_3 is expected, but it is a weak scatterer, and hard to detect by XRD. A small amount of Fe_2O_3 was observed as a red color on the surface of the Al_2O_3 boat used for sintering the powder, which was also observed during the sintering of YFe_2O_4 **[Muller, 2012]** and $LuFe_2O_4$ **[de Groot, 2012].**

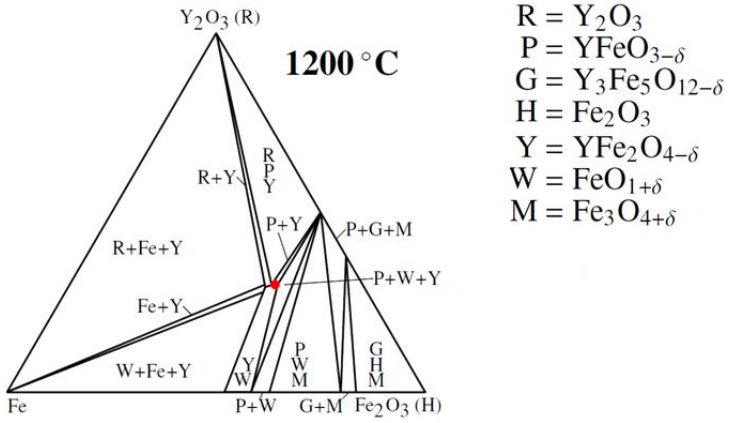

Figure 3.3 Phase diagram of the Fe-Fe_2O_3-Y_2O_3-system at 1200 °C. Reproduced by [Muller et al., 2015] from [Kimizuka and Katsura, 1975].

3.1.2 Oxygen-stoichiometry of $Lu_{0.5}Y_{0.5}Fe_2O_{4-\delta}$

3.1.2.1 Low-field magnetization results

Low field magnetization measurements are used for stoichiometry indication as discussed in the introduction. Therefore, after the range in which $Lu_{0.5}Y_{0.5}Fe_2O_4$ is a single phase was determined, the quality of the powder samples was assessed by low-field magnetization measurements using the VSM option of the PPMS or PPMS dyna-cool as described in section 2.1.2.

The temperature dependence of the magnetization (M vs. T) was measured under three modes: ZFC, FC, and FW. The measurements were conducted for temperatures in the range 10-300 K and the applied field was always 100 Oe. With these values, a magnetic characterization of the transition temperature range and sharpness in dependence on the stoichiometry can be achieved. The magnetization is calculated from the measured magnetic moment in Bohr magneton per formula unit (μB/f.u.). The errors in the measurements of samples masses yield an error in the magnetization of about $\pm 1.0 \times 10^{-5}$ μB/f.u.

Figure 3.4 (left panel) shows the low-field magnetization measurements of the first prepared polycrystalline sample S1 synthesized in a low oxygen concentration i.e. gas ratio (5:30). There is almost no difference between the FC and FW curves, and they exhibit a very broad transition at approximately 200 K. The very broad peak with a large ZFC-FW difference at low temperature suggests a glassy magnetic behavior commonly observed for $RFe_2O_{4-\delta}$ samples with large off-stoichiometry δ **[Mueller, 2012] and [Williamson, 2012]**.

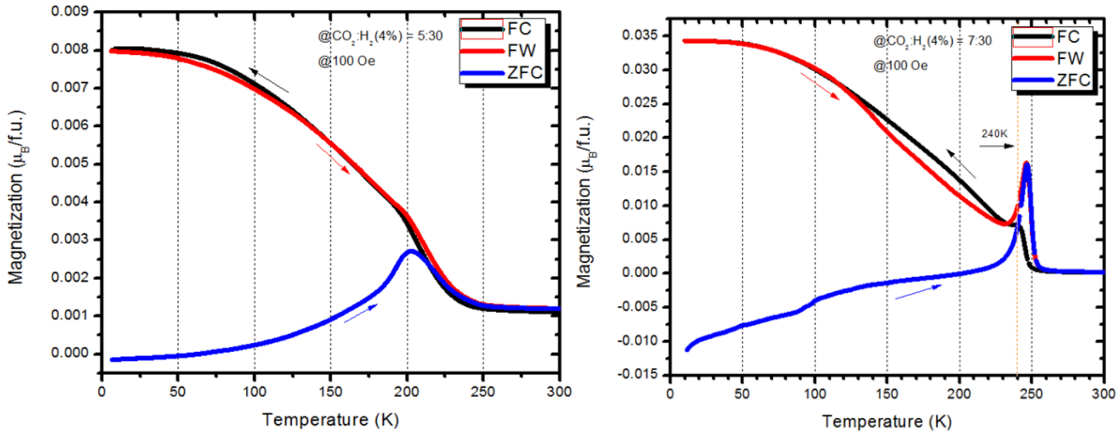

Figure 3.4 Temperature dependence of magnetization for (left) sample S1. (right) sample S2.

Sample S2 produced in an atmosphere with an increased gas ratio and consequently a higher oxygen partial pressure, exhibits a new magnetic behavior as shown in figure 3.4 (right panel) : A narrow peak is observed with a notable shift in temperature compared to sample S1. The peak indicates a transition occurring around 250 K, which is close to the transition temperature of both $LuFe_2O_4$ and YFe_2O_4. At the transition temperature, a large difference between the FC and FW curves is observed. The FW curve exhibits a large transition peak, which is in combination with the difference at lower temperatures between ZFC and FC, not just an indication for a glassy magnetic state, but a characterization of at least a partial transition to an **anti-ferro-magnetically (AFM)-ordered state.**

However, a large magnetization at 10 K after FC indicates the presence of a ferrimagnetic (fM) state, so probably there exists a fM/AFM mixture. The ZFC and the FW magnetizations reach the same maximum value at the transition temperature, but a large difference between them at very low temperature means that glassy magnetism is still present. The negative ZFC magnetization at low temperatures is probably due to the presence of a small residual magnetic field during cooling. The S2, S3, and S4 samples exhibit a similar magnetic behavior with only differences in the sharpness of the transition peaks where a sharper peak is noticed for the sample with higher gas ratio i.e. oxygen content.

Sample S5 exhibits an interesting feature shown in figure 3.5 (left panel) in which the FC curve exhibits the most sharp transition peak in comparison to the other samples. A large thermal hysteresis is noticeable at this transition since the ZFC shows a maximum peak around 250 K and the FC around 240 K. All polycrystalline samples were measured with a sweeping rate of 2 K/min, and only this sample shows such a large difference in the transition temperature during FC, so this large hysteresis is an intrinsic property of S5.This is a surprising result, given that the hysteresis at the magnetic transition is much smaller in $LuFe_2O_4$ **[de Groot, 2012].** A small ripple is apparent around 100 K that might be due to an additional low T transition similar as in $LuFe_2O_4$ **[Williamson, 2012]**.

S6 (see figure 3.5 right panel) shows almost the same behavior as S5 with a notable thermal hysteresis but with a reduction of the transition peak sharpness. In addition, the overall

magnetization is higher which indicates destabilization of the AFM phase. The small feature visible in the FC curve is an artifact at low temperature due to sample jumping.

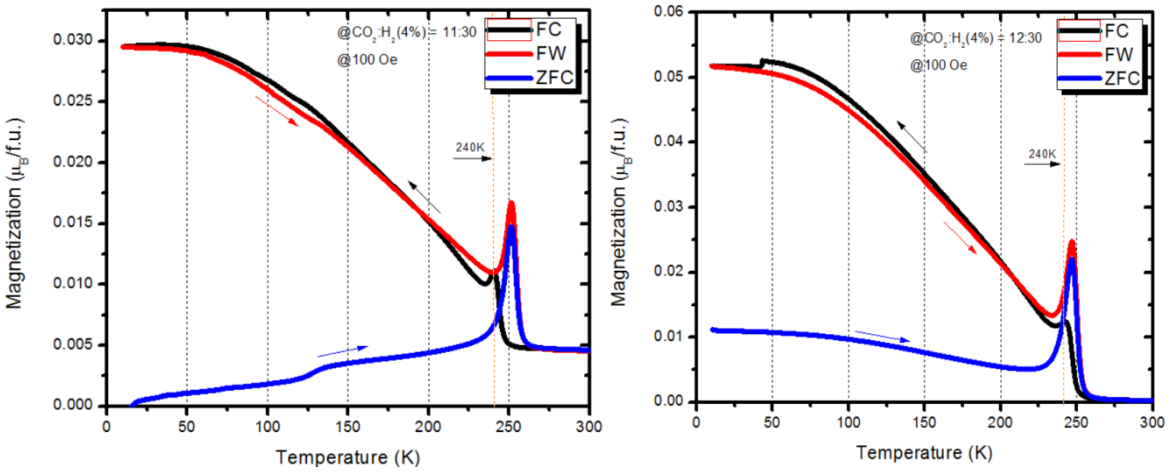

Figure 3.5: Temperature dependence of magnetization for samples S5 (left) and S6 (right).

3.1.2.2 Comparison of $Lu_{0.5}Y_{0.5}Fe_2O_{4-\delta}$ with $LuFe_2O_4$

In order to estimate the quality of the different $Lu_{0.5}Y_{0.5}Fe_2O_4$ polycrystalline samples, a comparison with $LuFe_2O_4$ samples with similar behavior was done. Studies on $LuFe_2O_4$ performed by **[Williamson, 2012]** on both single crystals grown under CO_2:CO =1:3 and 1:5 show a similar magnetic behavior to that of some of the polycrystalline $Lu_{0.5}Y_{0.5}Fe_2O_4$. The magnetization of the 1:5 crystal was measured, afterwards it was heated to 400 K for specific heat measurements, and then the magnetization was measured again.

Figure 3.6 shows the magnetization data from Williamson, in the left panel the 1:5 crystal and in the right panel the same crystal after heating to 400 K. A difference is notable in the magnetization. Both FC and ZFC of the 1:5 crystal before heating exhibit a very sharp transition peak at 234 K and another feature at lower temperature is observed in both FC and ZFC, while the FC of the premeasured one shows a less sharp peak. The 1:5 crystal is the most stoichiometric of Williamson's samples, however during the time it was at 400 K there was some slight change of the stoichiometry which might also be not completely homogenous since it is likely that vacuum annealing of a crystal will lead to a stronger decrease of the oxygen-content closer to the surface. But the sample is still relatively close to a stoichiometric one even after this change, because just a few hours at 400 K should not change the stoichiometry that much.

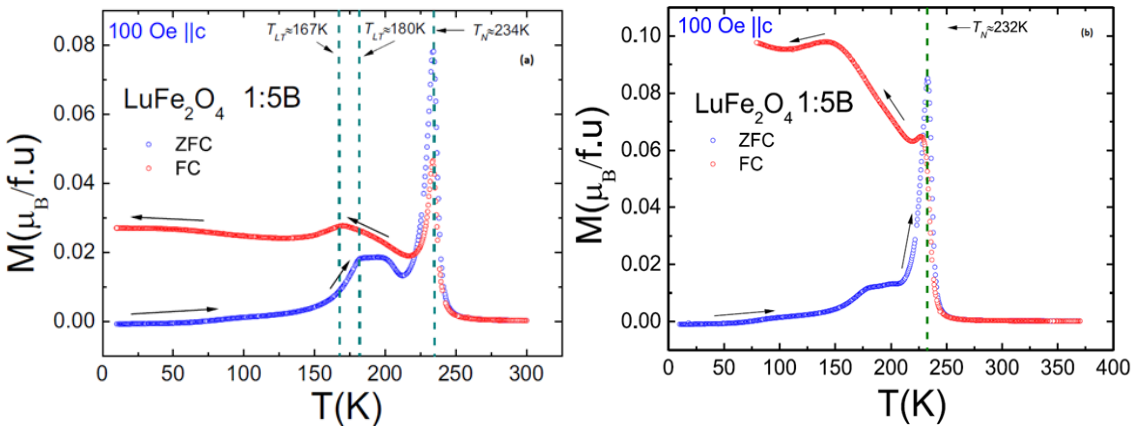

Figure 3.6: Magnetization M(T) of $LuFe_2O_4$ single crystals, measured under 100 Oe magnetic field for 1:5 crystal before (left), and after heating up to 400 K (right). [Williamson, 2012].

The magnetization of sample S5 (Figure 3.5) with the most sharp transition peak in the FC looks similar to that of the re-measured 1:5 crystal in the right panel, but with a slight shift in the transition temperature since the FC of sample S5 occurred at 240 K compared to 232 K for the re-measured crystal. One can conclude that S5 is slightly oxygen deficient, but quite close to ideal stoichiometry. There is a feature around 160 to 180 K visible only in the ZFC curve of the re-measured crystal and in both ZFC and FC curves in the measurement before heating, but this does not appear in any polycrystalline $Lu_{0.5}Y_{0.5}Fe_2O_4$ sample.

The low temperature feature does not necessarily link to the stoichiometry, since there are in the literature samples where this low temperature transition is completely suppressed even though that they have 3D magnetic order. For example, two samples of $LuFe_2O_4$ show sharp magnetic Bragg reflections in neutron scattering experiments, suggesting the existence of long-range magnetic order, although one of them exhibits such low temperature transition [**Wen et al., 2010**] and the other not **[Wen et al., 2009]**.

Another similarity in the magnetic behavior was observed between the crystal synthesized in a gas ratio of 1:3 shown in figure 3.7 and the polycrystalline S1 with gas ratio 5:30. The transition for both occurred at the same temperature around 200 K with no thermal hysteresis, but the $LuFe_2O_4$ crystal exhibits a narrower peak and a much higher maximum magnetization compared to the polycrystalline sample S1. Williamson's crystal was classified as having a poor stoichiometric quality based on both specific heat and X-ray diffraction **[Williamson, 2012]**. However, the stoichiometry of the crystals grown by Williamson is still

better than that of the polycrystalline sample S1, which is therefore quite far away from the ideal stoichiometry.

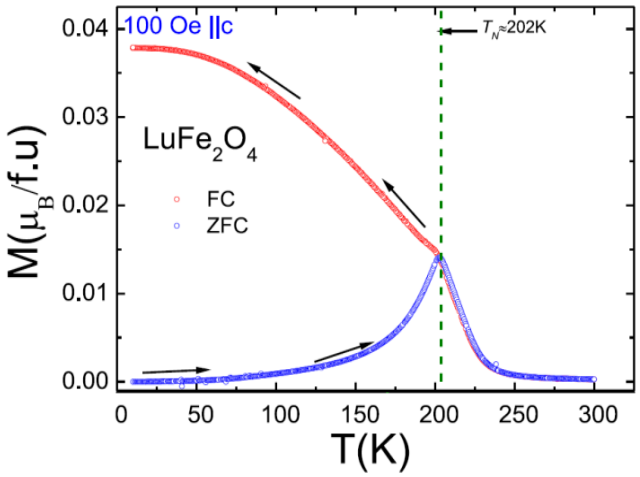

Figure 3.7 The magnetization M (T) of single crystal $LuFe_2O_4$ prepared under gas ratio 1:3, measured with an applied magnetic field of 100 Oe. Taken from [Williamson, 2012].

In the same year, **[de Groot et al. 2, 2012]** measured the magnetization of a good quality single crystal of $LuFe_2O_4$. Figure 3.8 shows the magnetic behavior for two crystals from the same growth measured during cooling with an applied field of 100 Oe.

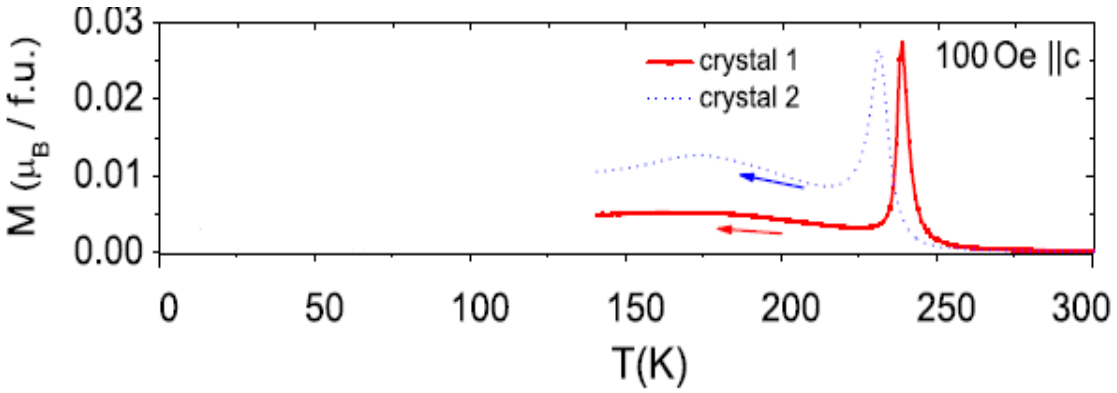

Figure 3.8 The magnetization (M) plotted vs. temperature (T) of $LuFe_2O_4$ single crystals measured with an applied magnetic field of 100 Oe. Reproduced from [de Groot et al. 2, 2012].

The FC curve of the crystal shown in the red solid line is classified to represent the best behavior based on the sharpness of the transition peak, while the FC curve of the other crystal with reduced sharpness indicates sample with a lower oxygen stoichiometry represented by the dashed blue curve. So one can conclude that the sharper the peak is the better quality is, confirming that the polycrystalline sample S5 has the best quality close to the stoichiometric one.

An older measurements done on $LuFe_2O_4$ by **[Wang et al., 2009]** shown in figure 3.9 (left panel) shows as well a similar magnetic behavior to that of the best quality sample S5 (right panel), with a shifting of the ZFC maximum to 250 K. However, the FC looks slightly better for Wang's measurements ,which has an oxygen excess. According to TGA, it is $LuFe_2O_{4.07\pm0.03}$ **[Wang et al., 2009].**

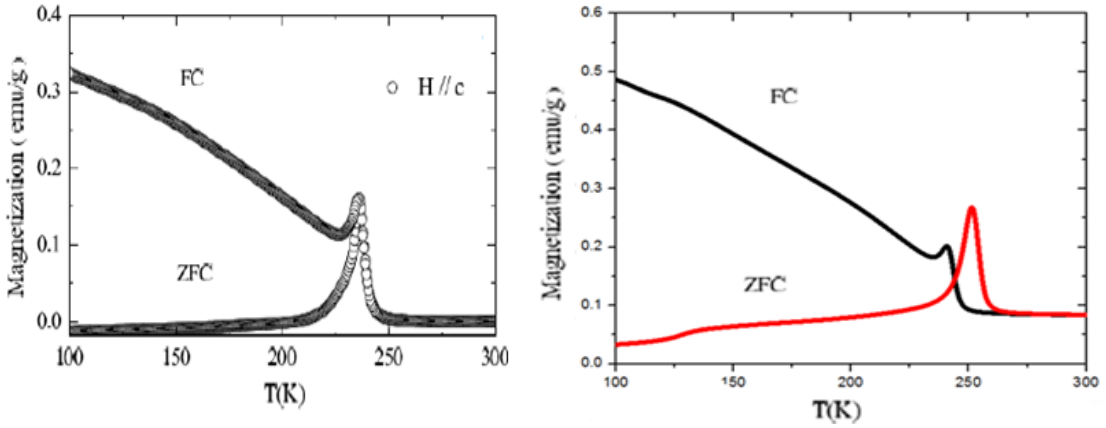

Figure 3.9 ZFC and FC magnetization in external fields of 10 Oe for measured (left panel) single crystal $LuFe_2O_4$ Wang's sample. Reproduced by [Williamson, 2012] from [Wang et al., 2009]. (Right panel) polycrystalline S5 $Lu_{0.5}Y_{0.5}Fe_2O_4$ measured with 100 Oe.

No previous measurements on substituted single crystals like $Lu_{0.5}Y_{0.5}Fe_2O_4$ have been published, and only a few on polycrystalline ones. Of these, measurements one was conducted by **[Serrao et al., 2008]** without any remarks on the stoichiometry on a pellet of $Lu_{0.5}Y_{0.5}Fe_2O_4$. This pellet was heated in an evacuated quartz tube at 1100 °C for 24 h and was afterwards quenched into liquid nitrogen, i.e. synthesized under completely different conditions in which S6 was prepared. The ZFC and FC measurements of Serrao's sample are shown in figure 3.10 (a) and the magnetic behavior of sample S6 is shown in figure 3.10 (b).

Serrao's polycrystalline sample exhibits a somewhat similar behavior as sample S6. Both FC and ZFC show only one main transition around 250 K. However, S6 exhibits a sharper peak indicating a higher stoichiometry. Therefore, for the polycrystalline S6, M(T) is much better than for the sample of **[Serrao et al., 2008].**

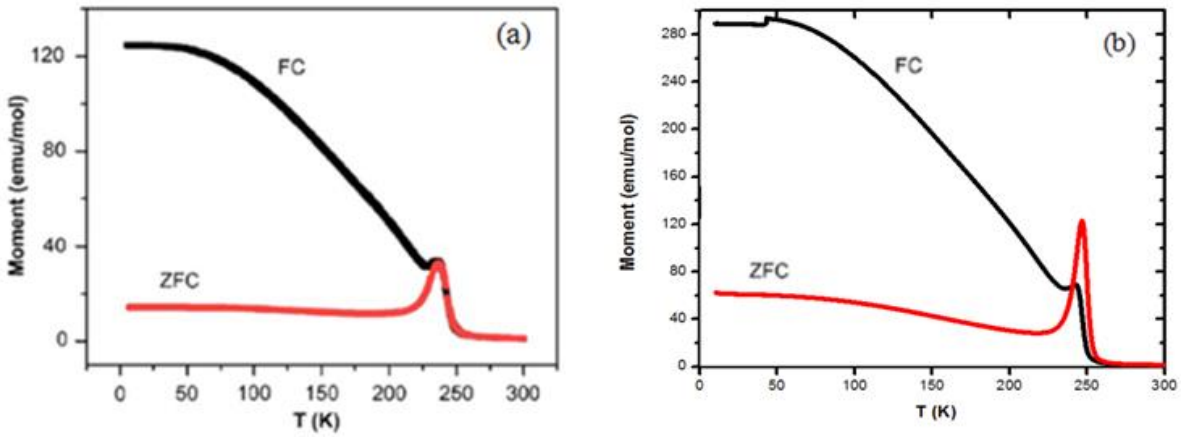

Figure 3.10 ZFC and FC magnetization measured for polycrystalline $Lu_{0.5}Y_{0.5}Fe_2O_4$ in an external field of 100 Oe (a) Serrao's sample. Taken from [Serrao et al., 2008]. (b) S6 sample.

The magnetization of S6 was measured with an applied field of 100 Oe and 1000 Oe. The magnetization measurements, which were done with an applied field of 100 Oe, show a clearly sharper transition than the measurements done with 1000 Oe. Therefore, our selection of low-field measurements was suitable and effective. This was expected from experience on $LuFe_2O_4$ **[de Groot, 2012]**. The magnetic behavior of S6 with an applied field of 1000 Oe is shown in figure 3.11.

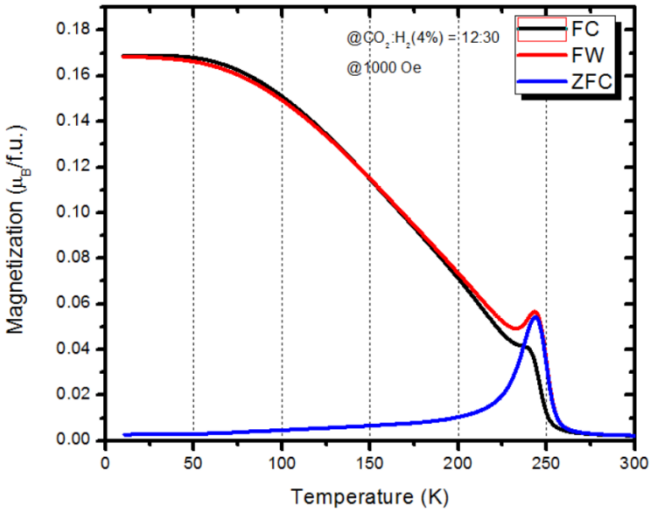

Figure 3.11 Magnetization measurements of sample S6 with an applied field 1000 Oe.

3.1.2.3 TGA results

TGA was used to calculate the deviation from the ideal oxygen-stoichiometry for different polycrystalline $\mathbf{Lu_{0.5}Y_{0.5}Fe_2O_{4-\delta}}$ samples. Both dynamic and isothermal modes are used through these measurements.

An amount of 20.200 mg from sample S1 was prepared under a low oxygen partial pressure. It was placed in the Al_2O_3 pan of the microbalance with 1 μg sensitivity in a furnace under a flow of reducing gas mixture Ar/H_2 (4%). The sample was heated in this reducing gas from room temperature up to 800 ˚C at a rate of 20 ˚C/min, and then heated to 1200 ˚C at a rate of 2 ˚C/min. It was kept there for roughly 1 hour, and finally was cooled down to RT at a rate of 20 ˚C/min. Figure 3.12 shows the percentage of the mass difference and the programmed temperature profile of sample S1.

The measurements of the mass difference were recorded by the TGA and for a crosscheck were done by an external balance. Table 3.2 shows the two measurements and the yielded values for δ and hence the stoichiometric formula.

Method	Δm (mg)	δ	Absolute error	Composition
TGA balance	**2.6260**	**0.00048**	**0.003**	**$Lu_{0.5}Y_{0.5}Fe_2O_{3.9995(30)}$**
External balance	**2.68**	**-0.0627**	**0.019**	**$Lu_{0.5}Y_{0.5}Fe_2O_{4.0627(19)}$**

Table 3.2 Measuring composition for sample S1.

The 54-μg difference between the TGA and the external balance is significantly larger than the error bar of both balances. It corresponds to a difference in δ of 0.05 and this is significant. It is important to note in this connection that for $\mathbf{YFe_2O_{4-\delta}}$ an off-stoichiometry δ = 0.03 already has a significant impact on the magnetization **[Inazumi et al., 1981].**

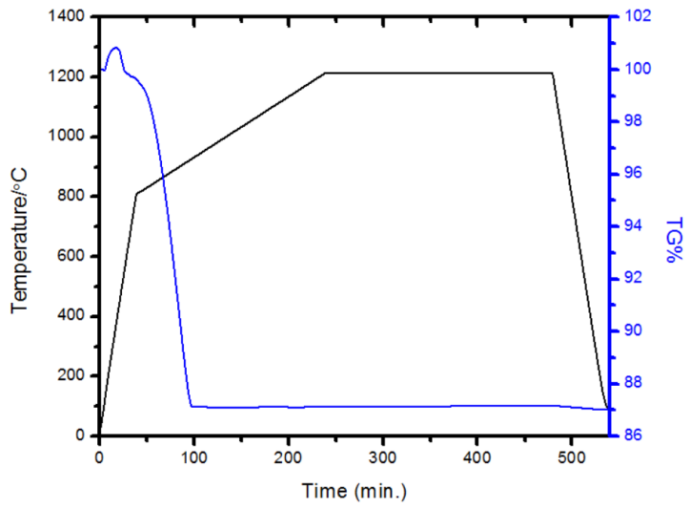

Figure 3.12 Mass difference percentage and temperature programming curves obtained from TGA for polycrystalline S1.

In calculating δ, I started with the absolute value of the mass difference recorded by the TGA balance, but a starting mass is needed to get the relative value needed in the equation

in section 2.2.3 which is usually done for external balance. With this $\delta = 0.00048$ (absolute error 0.003) and the composition will presumably be $\mathbf{Lu_{0.5}Y_{0.5}Fe_2O_{3.9995(30)}}$.

For crosscheck measurement, the end-value was measured by a less accurate external balance and the received value was very different. This lead to $\delta = -0.0627$ with an absolute error of 0.019, i.e. $\mathbf{Lu_{0.5}Y_{0.5}Fe_2O_{4.0627(19)}}$.

The two measurements were made with difference in the exposure to for short time in the reducing atmosphere at 30 °C. Here two scenarios are possible explaining the different results : Either the sample changed its stoichiometry during this short time at 30 °C, in this case, the δ calculated from the external balance would be more accurate, or adsorbed water was removed, and thus the TGA mass difference is appropriate. However, given that the starting mass is unreliable, I used the final mass from the external balance for scaling, which lead to $\delta = -0.0077$ with an absolute error of 0.0003, giving the composition $\mathbf{Lu_{0.5}Y_{0.5}Fe_2O_{4.0077(30)}}$.

Sample S1 exhibits a glassy magnetic behavior indicating that the sample is far away for the ideal stoichiometry and from comparison with other curves one can conclude that it is oxygen-deficient. The calculations based on the external balance indicate that the sample has an oxygen excess, which is unlikely according to magnetization measurements. However, even for the other small δ values, the oxygen deficit is too low to explain the magnetization measurements.

Of course, given the small statistical error bars, there must be systematic errors since the lowest oxygen stoichiometry found by TGA is $\mathbf{Lu_{0.5}Y_{0.5}Fe_2O_{3.9995(30)}}$, that would be as stoichiometric as the best $\mathbf{YFe_2O_4}$ samples **[Inazumi et al., 1981]**. Considering the magnetic behavior this cannot be true, therefore, the TGA measurement can only give us a relative orientation between different samples, but not an absolute value of the stoichiometry.

Sample S10, has two impurities determined as $Lu_{0.5}Y_{0.5}FeO_3$ and FeO. The measurement was made using the same reducing gas but with a different temperature profile (see figure 3.13) in which the sample was heated from RT to 1200 °C with a rate of 2 °C/min. Then it was kept at 1200 °C for roughly 4 hours and finally was cooled down to RT at a rate of 2 °C/min. The mass loss recorded by the TGA balance was 2.8110 mg, while measuring the

sample before and after the TGA run with an external balance gave 2.87 mg. The 59-μg difference in the TGA and external balance measurements is significantly larger than the error bar of both balances. Table 3.3 shows the net calculation for sample S10.

Method	Δm (mg)	δ	Absolute error	Composition
TGA balance	**2.8110**	**-0.00278**	**0.0025**	**$Lu_{0.5}Y_{0.5}Fe_2O_{4.0027(25)}$**
External balance	**2.87**	**-0.0674**	**0.018**	**$Lu_{0.5}Y_{0.5}Fe_2O_{4.067(18)}$**

Table 3.3 Composition Measurements for Sample S10.

The off-stoichiometry was calculated by three different methods for the 5:30 sample S1. The TGA difference gave δ = -0.00278 with an absolute error of 0.0025, so the composition **$Lu_{0.5}Y_{0.5}Fe_2O_{4.0027(25)}$**, while the mass difference measured by the external balance gave δ = -0.0674 with absolute error of 0.018, so the composition **$Lu_{0.5}Y_{0.5}Fe_2O_{4.067(18)}$**. In contrast, the third method with scaling the starting mass gave δ = -0.01119 with absolute error of 0.0025, so the composition **$Lu_{0.5}Y_{0.5}Fe_2O_{4.01119(25)}$.**

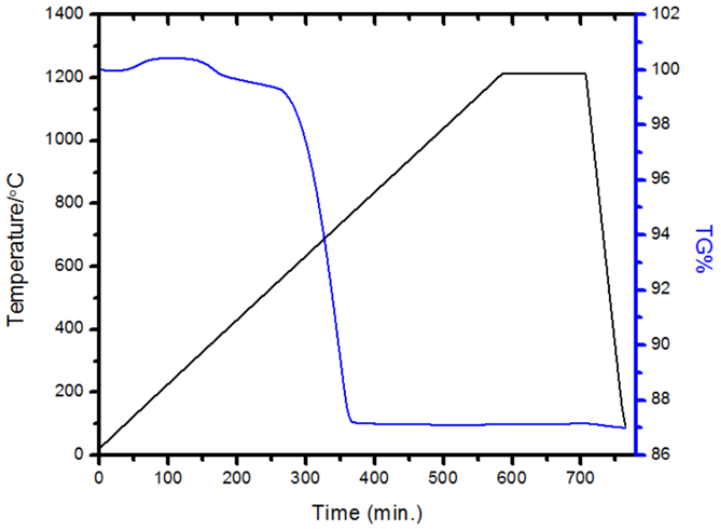

Figure 3.13 Mass difference percentage and temperature programming curves obtained from TGA measurements for polycrystalline S10.

Sample S10 shows impurities of both FeO and $Lu_{0.5}Y_{0.5}FeO_3$. Taking into account it was prepared in a high oxygen partial pressure indicates it has indeed an oxygen excess. At least all the calculated δ values shifted in compliance with the synthesis conditions, so the systematic errors seem to be independent of δ. The most reliable oxygen stoichiometry is δ = -0.0111(25) giving **$Lu_{0.5}Y_{0.5}Fe_2O_{4.0111(25)}$** which is close to the available $YFe_2O_{4-\delta}$ compound with the maximal oxygen content is YFe_2O_4 **[Kimizuka and Katsura 1, 1975]**, as well to

the Yb compound with **$YbFe_2O_{4.052}$ [Kimizuka and Katsura 2, 1975]** and to **$LuFe_2O_{4.015}$ [Sekine and Katsura, 1976]**.

3.1.3 Magnetic phase diagram

In this section, the magnetic properties of the best sample (S5) were investigated by measuring the magnetization Vs. the magnetic field. For the sharp transition at T~240 K, the isothermal magnetization M(H) was measured. No hysteresis behavior was observed at 230 K (see figure 3.14 upper panel). A very week hysteresis as observed at slightly lower temperatures and a significant hysteresis starts to emerge around 200 K.

The sample was cooled in zero magnetic field before the measurement to obtain the virgin (initial magnetization) curve. Therefore, no magnetization should be present because both spin up and spin down domains are compensating each other. Now for measuring the virgin curve, an external field was increased and thus the curve end with all domains aligned up.

As we started with an equal distribution between spin up and spin down domains configuration with applying a positive field, a higher magnetization will be produced compared to a start with all spins down, resulting in virgin curve inside the hysterics loop, regardless if there is hysteresis or not. However, this is not the case as shown in figure 3.14, which shows the isothermal magnetization of the sample S5 at different temperatures. The virgin curve is observed outside the hysteresis loop. **The only way to explain this behavior is to assume that two different phases are stabilized in the high and the low fields.**

The high H phase, represented by the segments (2-5) has a net moment, which seems similar to that of $LuFe_2O_4$ **[de Groot at al. 2, 2012]** indicating a ferrimagnetic phase, while the low H phase has zero net moment indicating an AFM phase. This feature suggests a **first order metamagnetic transition** which means both antiferromagnetic (AFM) and ferriemagnetic (fM) phases can be stabilized at H =0.0. This means there is a hysteresis in the phase transition between the AFM and fM phases. Applying a magnetic field higher than the coercive field, will trigger a transition from the AFM phase to the fM phase, but with decreasing the field to zero or even to a negative value, the AFM state cannot be reached.

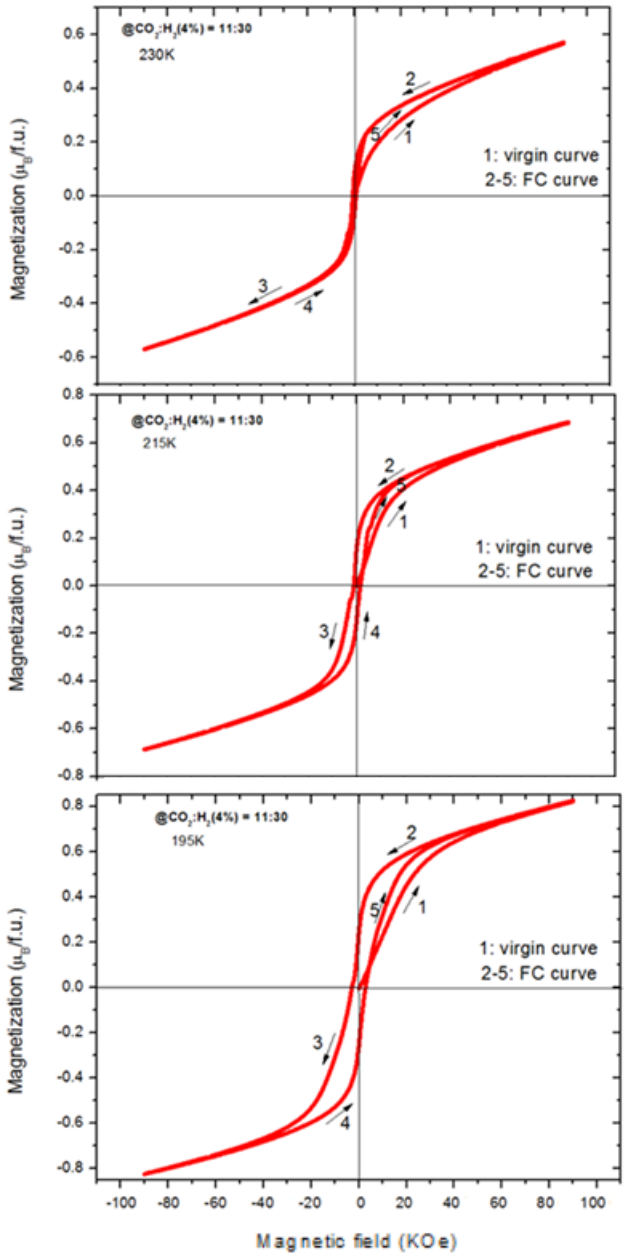

Figure 3.14 M(H) curves of Sample S5 at different temperatures.

The only possibility to reach it, is to heat the sample above the Neel temperature and cool down again in zero-field. Very similar behavior was noticed in $LuFe_2O_4$ first by **[de Groot et al. 2, 2012]** in the best quality crystal confirming that our powder is close to stoichiometry. The H-T phase diagram of $LuFe_2O_4$ extracted from de Groot's measurements is shown in figure 3.15. Note that a met magnetic transition is absent in YFe_2O_4 **[Mueller, 2012]**. However, in contrast to the phase diagram by **[de Groot et al. 2, 2012]**, one can see that for

S5 there is no region where only the AFM phase is stable –even cooling in zero field renders a part of the sample ferrimagnetic, consistent with the small drop of M upon cooling in low H (Figure 3.5 left panel).

The similarity of the met magnetic transition present in (enough stoichiometric) $LuFe_2O_4$, but absent in YFe_2O_4 lead to the expectation of a spin order very similar to $LuFe_2O_4$ as expected according to Kishi's measurements.

Magnetization measurements as a function of the magnetic field reveal that above 240 K a paramagnetic phase is present, below 240 K no hysteric behavior down to 225 K is observed, and the virgin curve behavior in the hysteresis loop reveals that competing antiferromagnetic (AFM) and ferrimagnetic (fM) spin structures can be stabilize.

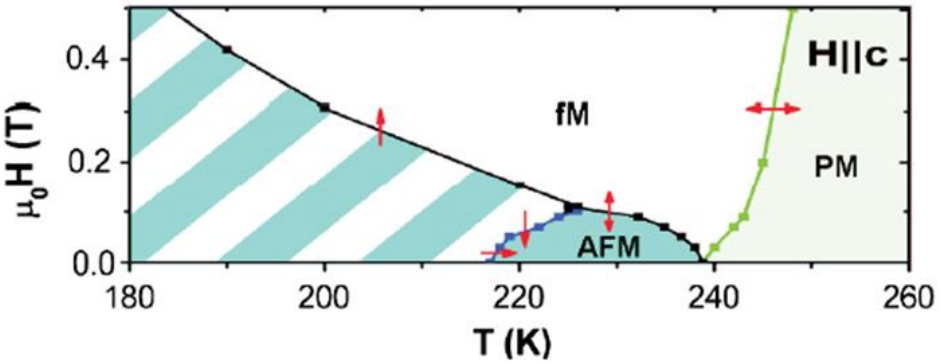

Figure 3.15 H-T phase diagram of $LuFe_2O_4$. Taken from [de Groot et al. 2, 2012]. In the hatched region, the AFM phase is stable when reached by increasing H after zero-field cooling and the fM phase is stable when reached by decreasing the field from high values.

3.2 Single crystals $Lu_{0.5}Y_{0.5}Fe_2O_{4-\delta}$

After the high quality stoichiometric powder was synthesized, a first trial of a crystal growth was started, followed by an optimization of the growth parameters to obtain a stoichiometric single crystal. All crystals were grown by the floating zone method using a mirror furnace under different CO_2-CO gas ratios. The following table shows the growth parameters : The used gas ratio, the used power and the obtained growth lengths. G1 indicates the first growth, G2 the second growth and so on. All crystals were grown with a speed of 1 mm/hour **[Shindo et al., 1976]**.

Name	CO_2/CO	Power(%)	Growth length (mm)
G1	2.94	40	-
G2	4.95	44.1	26.4
G3	6.28	44.5	25.3
G4	7.07	43.4	18.4
G5	7.85	42.5	23
G6	9.42	44.1	18.7
G7	7.46	43.7	26.5
G8	6.44	43.6	40

Table 3.4 Various single crystal growth parameters of $Lu_{0.5}Y_{0.5}Fe_2O_{4-\delta}$.

Figure 3.16 (left side) shows the grown rod on the top of the polycrystalline seed rod of the second growth G2, the shiny part corresponds to the crystalline $Lu_{0.5}Y_{0.5}Fe_2O_{4-\delta}$. The grown rod, which typically contains a considerable number of relatively small single crystals, was crushed by a hammer to obtain small crystals suitable for magnetization measurements.

Laue diffraction is used for crystal orientation. The orientation of crystal was changed until a hexagonal symmetry shown in figure 3.16 (right side) is obtained which indicate that hexagonal c-axis is aligned paralleled to the beam. The sample is not a single crystal since reflections not belonging to the hexagonal pattern are observed (marked with arrows).

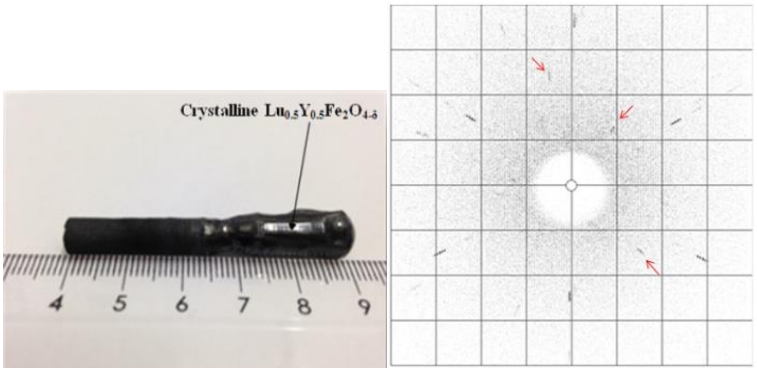

Figure 3.16 Picture of second growth G2 (left side). Laue diffraction of crystal perpendicular to c-axis at RT (right side).

After each crystal growth, the crystals were analyzed by powder XRD, magnetization measurements and even by optical microscopy in order to fine-tune the oxygen partial pressure. Powder XRD was used to check the phase purity, and it was an indication for the oxygen partial pressure as well, since foreign phases are likely to occur with increasing oxy-

gen pressure (see section 3.1.1). Low-field magnetizations measurements were performed as an indication of the oxygen-stoichiometry, especially after the magnetic behavior of stoichiometric polycrystalline samples was known, it was straightforward to determine the quality of the crystals.

3.2.1 Magnetization measurements

For both YFe_2O_4 **[Mueller et al., 2015]** and $LuFe_2O_4$ **[de Groot, 2012]**, different magnetic behaviors were observed for different crystals from the same growth, which indicates that the crystal position influences the stoichiometry. This is expected for $Lu_{0.5}Y_{0.5}Fe_2O_4$, and therefore three crystals from different positions along the grown rod for each growth were checked by magnetization measurements using the same procedure and conditions as described before.

A large anisotropy is reported for $LuFe_2O_4$ and the easy axis is along the c-axis **[Wang et al., 2009],** because the Fe spins are preferred to aligned perpendicular to the layer i.e. in c-direction **[Iida et al., 1986]**, therefore the M(T) measurements were done on the crystals with a field of 100 Oe applied along the c-axis. In all used magnetometers, the field is parallel to the probed component of the magnetization.

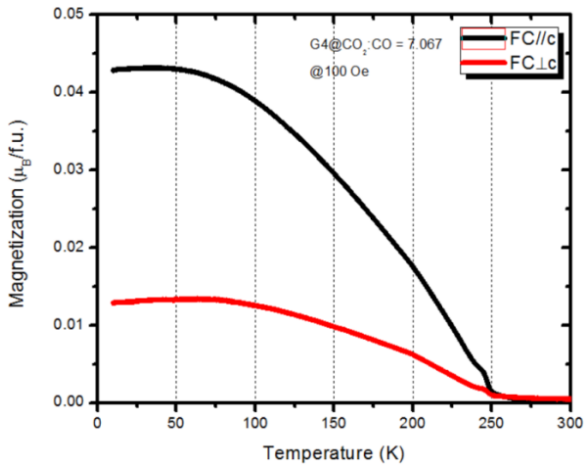

Figure 3.17 Temperature dependence of the magnetization of the crystal from the lower part of the G4 growth measured with an applied field of 100 Oe parallel or perpendicular to the c-axis.

Figure 3.17 shows the temperature dependence of the magnetization (FC) of single crystalline $Lu_{0.5}Y_{0.5}Fe_2O_4$ which was grown under the gas ratio 7.07 (see Table 3.2) obtained with a field of 100 Oe applied parallel or perpendicular to the crystallographic c-axis. This

measurements confirm that this compound is not isotropic since the magnetization in the field is parallel to the c-axis about 4 times larger than the magnetization of the perpendicular alignment. However, this ratio is not as large as expected, which might be due to a non-ideal alignment of the sample about the field.

After we know the magnetic behavior of the best quality polycrystalline sample, a comparison with this sample would be beneficial to evaluate the quality of the crystals. Figure 3.18 (left panel) shows the FC curves of different polycrystalline samples prepared under different gas ratios CO_2:H_2 (4%), while figure 3.18 (right panel) shows the FC curve of different single crystals prepared under different CO_2:CO ratios. For some growths, the magnetization measurements were done on many crystals from the same batch. In the legend, T refers to crystals from top part of grown rod, M to middle and B to bottom part. The magnetic behavior of the crystals was not as good as for the polycrystalline samples, since none of the FC curves shows a sharp peak as observed in the high quality powder sample.

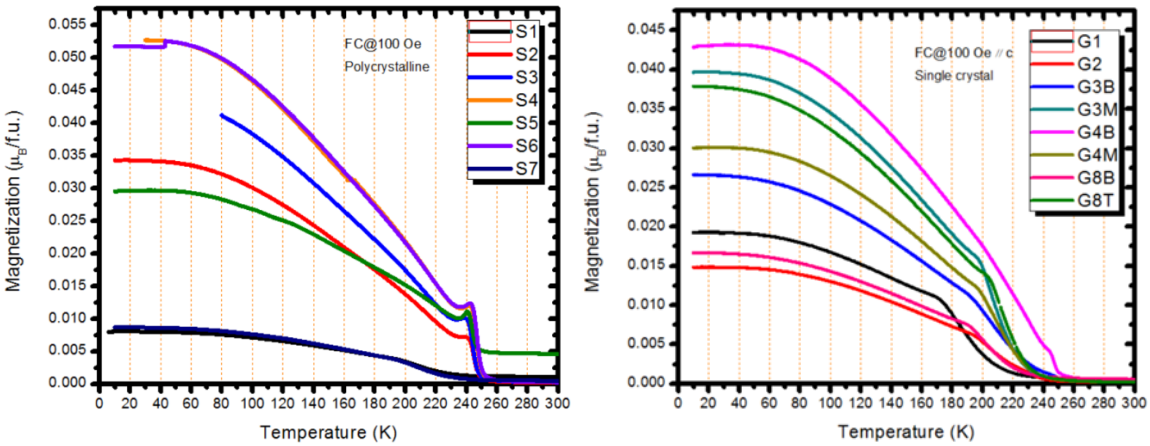

Figure 3.18 Temperature dependences of the FC magnetizations M(T) for polycrystalline $Lu_{0.5}Y_{0.5}Fe_2O_4$ (left panel) and for single crystals $Lu_{0.5}Y_{0.5}Fe_2O_4$ (right panel).

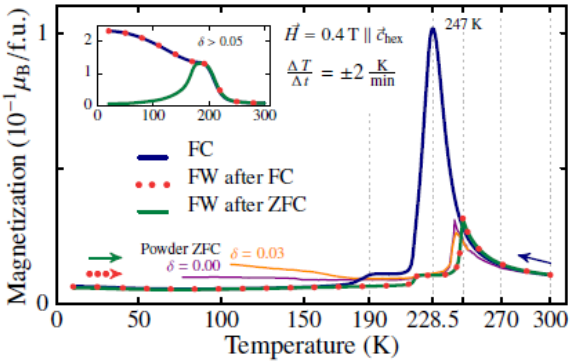

Figure 3.19 Magnetization measurements of both stoichiometric and non-stoichiometric YFe_2O_4 single crystal. Taken from [Mueller et al., 2015].

In addition, all polycrystalline samples except S1 and S7 showed a sharp peaks, and steep rise between 240 K and 250 K. For the crystals only G4B measurements showed noticeable behavior. Based on the observations in YFe_2O_4 (figure 3.19) **[Mueller, 2012]**, The abrupt increase of the transition temperature in combination with the onset of a peak in the magnetization for G4B, indicate an increased stoichiometry, approaching the perfect values.

3.2.2 Charge order

No investigation of the charge order of single crystalline or even polycrystalline $Lu_xY_{1-x}Fe_2O_{4-\delta}$ by any diffraction technique is reported. The CO of a few selected crystals was probed by single crystal X-ray diffraction, from which a map of scattered intensity in reciprocal space is obtained (see section 2.2.1.3). Single crystal diffraction measurements were done on two crystals G1 and G4 at room temperature and at low temperatures.

Figure 3.20 shows the projections of the reciprocal hhℓ plane for the crystal G1 at RT (left panel) and 160 K (right panel). The G1 crystal exhibited very weak diffuse lines along (1/3, 1/3, ℓ) and (2/3, 2/3, ℓ) in addition to Bragg reflections from the R$\bar{3}$m structure as was discussed in section 2.2.1. After cooling to 160 K, these diffuse lines became stronger.

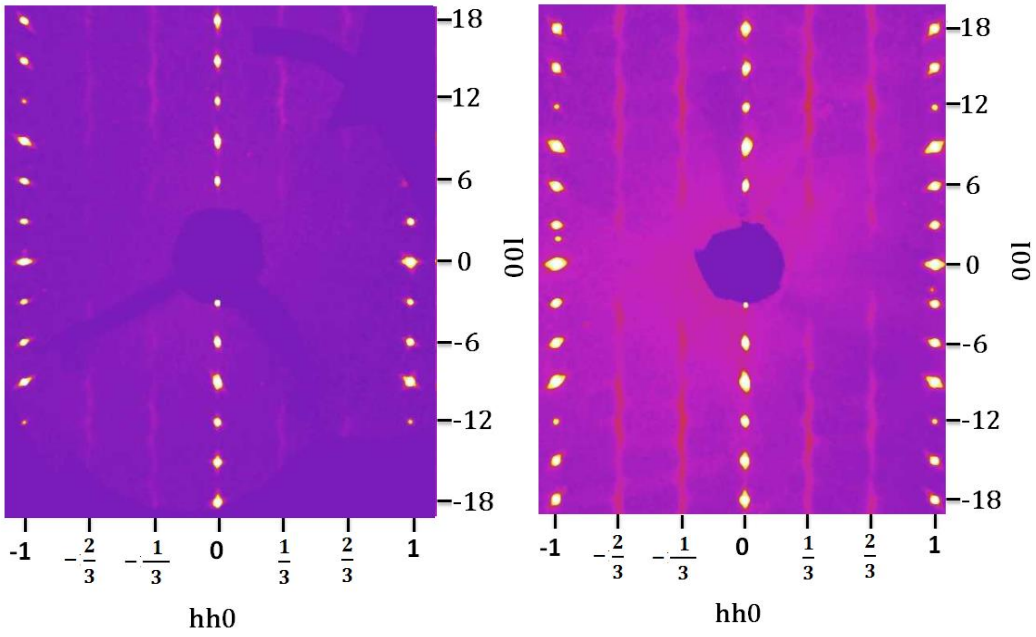

Figure 3.20 Precession image in the hhℓ plane from single crystal X-ray diffraction for the crystal G1 at 300 K (left side) and 160 K (right side).

Figure 3.21 shows the projection of the reciprocal hhℓ plane for the crystal G4 at 100 K. This crystal shows diffuse lines at both RT and 100 K, confirming that the crystal is non-stoichiometric.

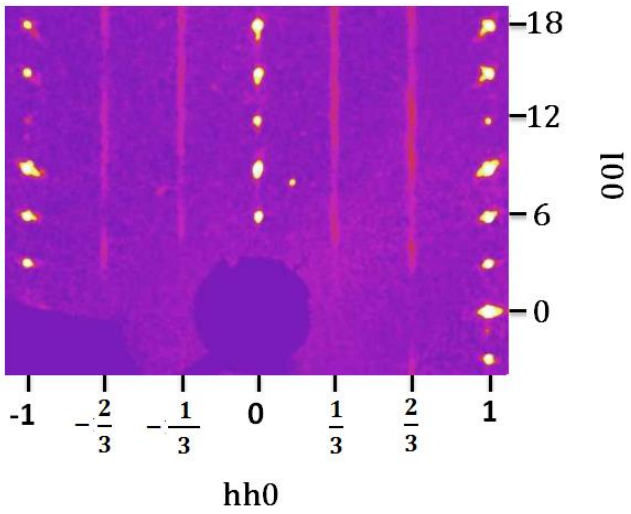

Figure 3.21 Precession image in the hhℓ plane for the crystal G4 at 100 K.

The CO in figure 3.22 leads to an increased cell (the dashed cell) including additional Bragg reflections. E.g. for Bragg planes perpendicular to [110], since the plane spacing d becomes three times larger, the Bragg equation mentioned in section 2.2.1 is additionally fulfilled for sinθ equal 1/3 of the values as that for (110).

However, the width of Bragg peaks is given by the average number of CO cells that are coherently ordered **[Angst, 2015]**. For a high number the corresponding Bragg reflections will be sharper than if we have a small number. Essentially the width of Bragg peaks is inversely proportional to the average sizes of the regions with CO. If this size is very small, a diffused line is observed instead of peaks. As the diffuse lines still have a relatively sharp profile in the hh0-direction that the coherently ordered CO regions are extended in the c-plane, whereas out of plane they do not extend beyond a single bilayer. This behavior is often found in non-stoichiometric $LuFe_2O_4$ **[Williamson, 2012]** and YFe_2O_4 **[Mueller, 2012].**

Diffuse scattering near (1/3 1/3 ℓ) and (2/3 2/3 ℓ) is observed for the two crystals at RT and even at lower temperature indicating only 2D CO. This is the same type of diffuse scattering observed at all temperatures for samples with significant oxygen deficiency as in off-stoichiometric $LuFe_2O_4$, $YbFe_2O_4$, and YFe_2O_4 **[Angst, 2013]**. This diffuse scattering of X-

rays at (1/3 1/3 ℓ) suggests a tendency towards a CO with a $\sqrt{3}\times\sqrt{3}$ cell shown in figure 3.22 or an equivalent C-centered monoclinic cell which is enlarged three times along its b-axis **[Angst, 2013].**

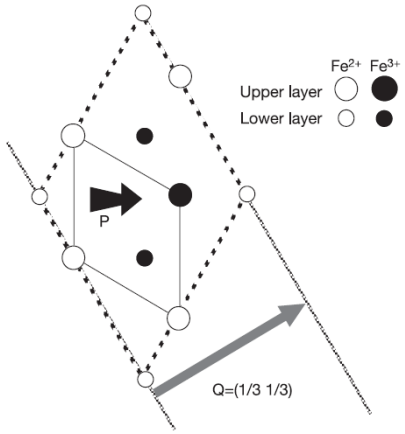

Figure 3.22 $\sqrt{3}\times\sqrt{3}$ cell CO as proposed by Ikeda. Taken from [Ikeda et al., 2005].

3.3 Polycrystalline $Lu_{0.1}Y_{0.9}Fe_2O_{4-\delta}$

Powder samples of $Lu_{0.1}Y_{0.9}Fe_2O_{4-\delta}$ were prepared under gas flows of different CO_2-H_2(4%) mixtures to control the stoichiometry as described in section 2.1.1. These samples are summarized in Table 3.3 with the used gas ratios.

Name	CO_2 (ml/min)	Ar-H_2(4%) (ml/min)	CO_2/H_2
A1	**5**	**30**	**4.17**
A2	**6**	**30**	**5**
A3	**7**	**30**	**5.83**
A4	**8**	**30**	**6.67**

Table 3.5 Different polycrystalline $Lu_{0.1}Y_{0.9}Fe_2O_{4-\delta}$ samples calcinated under different gas ratios.

3.3.1 Phase purity

All samples were checked by powder X-ray diffraction at room temperature to verify the presence of a single phase. $Lu_{0.1}Y_{0.9}Fe_2O_{4-\delta}$ contains 90% YFe_2O_4, therefore we compare its diffracto-gram with that of YFe_2O_4.

Figure 3.23 shows the comparison between the $Lu_{0.1}Y_{0.9}Fe_2O_{4-\delta}$ diffracto-grams with that of YFe_2O_4. A few impurities of both $Y_{0.9}Lu_{0.1}FeO_3$, and FeO appear in the A1 sample. Both are expected according to the YFe_2O_4 phase diagram (see figure 3.3). However, with increasing the gas ratio, these impurities appear more clearly and become larger.

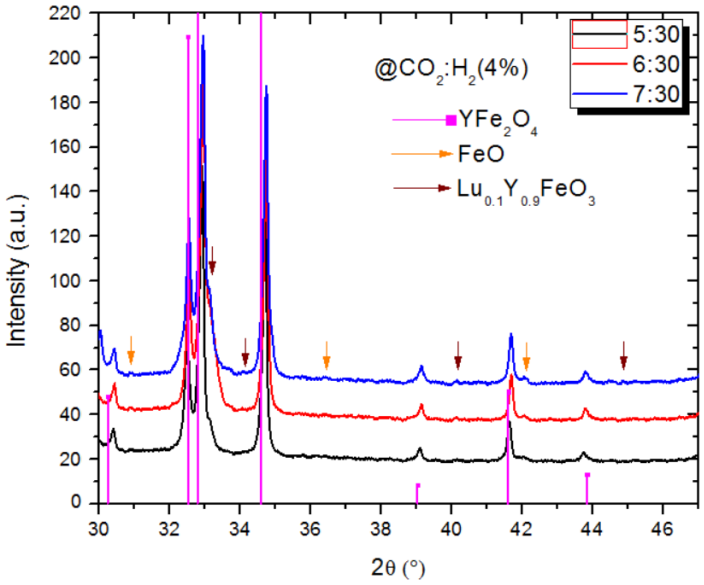

Figure 3.23 Comparison between powder XRD of $Lu_{0.1}Y_{0.9}Fe_2O_{4-\delta}$ samples and YFe_2O_4.

The optimum value of the gas ratio CO_2/H_2(4%) used to obtain stoichiometric YFe_2O_4 was 4.17 according to **[Mueller, 2012].** Therefore, it might be that the foreign phases, which occurred, indicate too much oxygen content. On the other hand, it might be due to the decomposition of YFe_2O_4 at 1100 ˚C **[Kitayama et al., 2004]** as the samples were cooled slowly during synthesis.

3.3.2 Low-field magnetization

The magnetization in low field was measured for the polycrystalline samples to check the oxygen-stoichiometry exactly as for $Lu_{0.5}Y_{0.5}Fe_2O_4$. ZFC, FC and FW modes were measured in the temperature range 10-300 K with a sweeping rate of 2 K/min and an applied field of 100 Oe. Figure 3.24 shows the low-field magnetization measurements of the first prepared polycrystalline sample A1, which was prepared at low oxygen partial pressure (gas ratio 4.17). Almost no difference between FC and FW is observed and the curve exhibits a very large broad peak at ~ 186 K, indicating a glassy magnetic behavior.

There is a feature observed around 120 K which is the Verwey transition **[Verwey, 1339]** due to contamination by magnetite, which is not expected from the YFe_2O_4 phase diagram at 1200 ˚C, so it may arise due to slow cooling of the sample inside the furnace, since the phase diagram looks different at different temperatures. However, the phase diagrams have been established only at two temperatures: at 1200 ˚C (Figure 3.3) by **[Kimizuka and**

Katsura, 1975] in which YFe_2O_4 is present as a stable phase and at 1100 ˚C (Figure 3.25) by **[Kitayama et al., 2004]**, where YFe_2O_4 is not present as a stable phase.

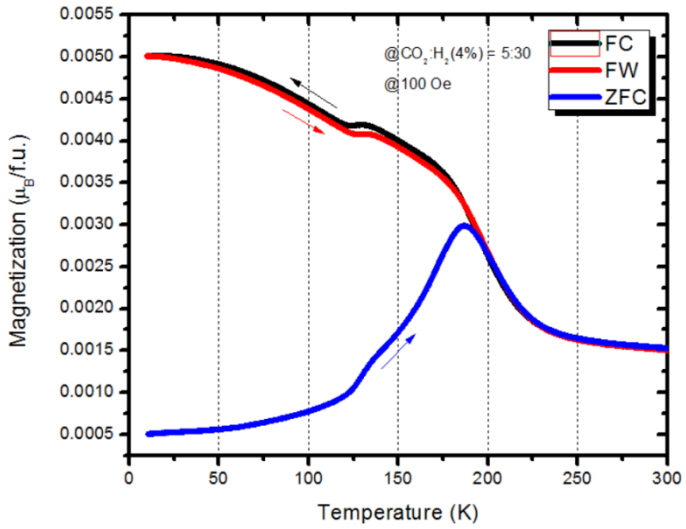

Figure 3.24 ZFC, FC and FW magnetization curves of sample A1 measured with a field 100 Oe.

In the 1200 ˚C phase diagram, no phase region containing YFe_2O_4 has a direct connection to regions containing magnetite. The region containing the mixture of Wüstite, YFe_2O_4 and $YFeO_3$ in the 1200 ˚C diagram however, correspond to a region that contains magnetite at 1100 ˚C. At lower temperatures, this region could extend even more. Therefore magnetite contribution can be explained through the cooling process. considering, that $LuFe_2O_4$ neighboring phases to $LuFe_2O_4$ contain magnetite **[Sekine and Katsura, 1976]**.

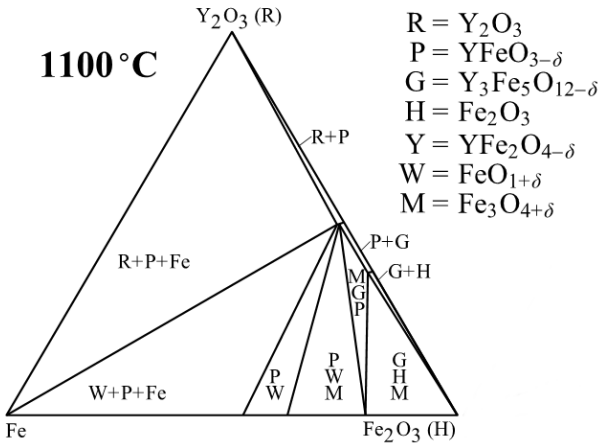

Figure 3.25 Phase diagram of the Fe-Fe_2O_3-Y_2O_3-system at 1100 ˚C. Reproduced by [Muller, 2012] from [Kitayama et al., 2004].

Upon increasing the gas ratio to (6:30), a notable shift in temperature is observed in all curves ZFC, FC, and FW, with a peak that occurs now at 200 K which indicates better stoi-

chiometry as shown in figure 3.26. The ZFC peak is narrower than in A1. A large difference is notable between FC and FW in which FC exhibits a sharper and higher peak than the corresponding FW curve.

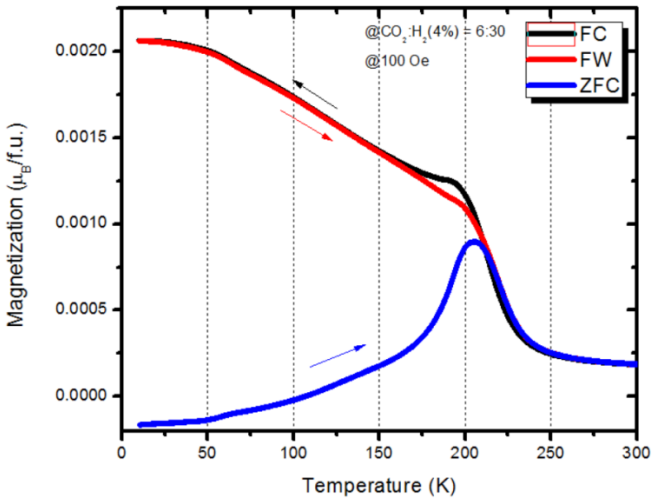

Figure 3.26 ZFC, FC and FW magnetization curves of sample A2 measured with an applied field 100Oe.

3.3.2.1 Comparison of $Lu_{0.1}Y_{0.9}Fe_2O_{4-\delta}$ with YFe_2O_4

As the composite consists of 90% Y and only 10% Lu, its magnetic behavior is compared with that for YFe_2O_4. Studies on polycrystalline YFe_2O_4 with off stoichiometry $\delta = 0.095$ performed by **[Inazumi et al., 1981]** and measured with an applied field of 3.97 kOe show a magnetic behavior similar to that of sample A1. Figure 3.27 shows the magnetic behavior of Inazumi's sample. Both samples have the same peak shape. Moreover, ZFC and FC show the same transition temperatures, and the drop afterward is very similar as well.

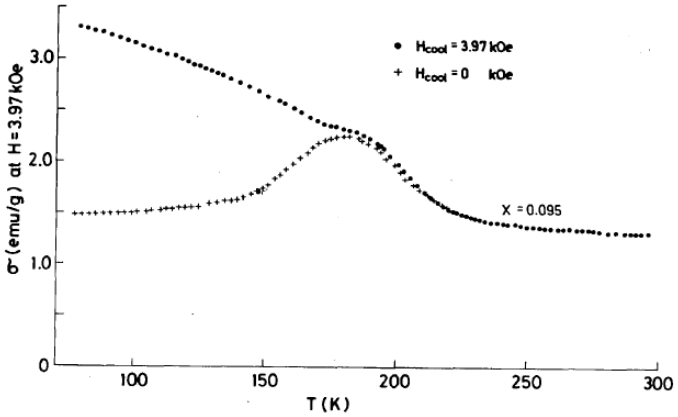

Figure 3.27 ZFC and FC magnetization of polycrystalline YFe_2O_4 measured with an applied field 3.97 kOe. Reproduced from [Inazumi et al., 1981].

However, compared to the A2 sample, it occurs at a slightly higher temperature indicating a higher stoichiometry, the shape is different although their transition peak appears at the same temperature, which might be an indication that the magnetic behavior of the substituted compound is distinct from YFe_2O_4.

3.3.2.2 Comparison of $Lu_{0.1}Y_{0.9}Fe_2O_{4-\delta}$ with $Lu_{0.5}Y_{0.5}Fe_2O_4$

Many polycrystalline $Lu_{0.5}Y_{0.5}Fe_2O_4$ samples show a transition peak around 250 K except for sample S1 where it is at 200 K. Therefore, the comparison of the magnetic behavior is done with the S1 sample (Figure 3.4 left panel).

The A1 sample exhibits a transition peak at a slightly lower temperature than S1 and the magnetization differs further as A1 is contaminated with magnetite. In contrast, A2 exhibits the same transition temperature. However, a difference between the FC and FW curves is observed in A2 as the FC exhibits a sharp peak and the corresponding FW curve a broad peak, but for S1 there is no difference observed between the FC and FW curves, and they exhibit a very broad transition. These un-similarities indicate that $Lu_{0.1}Y_{0.9}Fe_2O_4$ is not the same phase as $Lu_{0.5}Y_{0.5}Fe_2O_4$ with a different magnetic behavior.

3.3.2.3 Comparison of $Lu_{0.1}Y_{0.9}Fe_2O_{4-\delta}$ with previous measurements

Pervious measurements by **[Kishi et al., 1983]** on polycrystalline $Lu_{0.1}Y_{0.9}Fe_2O_{4+\delta}$ with δ = -0.014 were shown in figure 1.13. Both the FC and ZFC curve of these measurements exhibit a very sharp peak, which is different from both the A1 and A2 sample. The magnetic transition of Kishi's sample occurs around 240 K, which is higher than observed in our samples. Therefore, Kishi's samples have a different behavior than ours.

All the comparisons discussed are tentative, since no stoichiometric samples are available and it is quite necessary to prove that this high percentage Y composition has a different charge and spin orders than $LuFe_2O_4$ and YFe_2O_4.

4

Summary and Future Work

4.1 Conclusions

This thesis is the first step to systematically study the effect of the rare earth ion size on the ordering processes in geometrically frustrated rare earth ferrites RFe_2O_4 by partially substituting Y (larger ion size) by the smaller Lu i.e. $Lu_xY_{1-x}Fe_2O_4$. Two compositions were studied during this thesis, x=0.5 and 0.1.

4.1.1 Measurements on $Lu_{0.5}Y_{0.5}Fe_2O_{4-\delta}$

A close to ideal stoichiometry for the polycrystalline $Lu_{0.5}Y_{0.5}Fe_2O_4$ samples was achieved for the first time. The magnetic behavior with only one main transition around 250 K contrasts with the behavior of YFe_2O_4 but shows strong similarity to $LuFe_2O_4$ behavior.
Competing AFM-fM magnetic phases were noticed through isothermal magnetization measurements on the high stoichiometry polycrystalline sample, similar to $LuFe_2O_4$ confirming the similarities in the magnetic behavior.

Single crystals of $Lu_{0.5}Y_{0.5}Fe_2O_{4-\delta}$ were grown by the floating zone method using a mirror furnace under different CO_2/CO gas flows, their magnetic behavior was not as good as for the best polycrystalline samples, and single crystal XRD showed 2D charge order with diffuse scattering along (1/3 1/3 ℓ) even at low temperatures indicating that the crystals are not stoichiometric enough. Therefore further optimization is needed to verify that the charge and spin structures are indeed identical to $LuFe_2O_4$, indicated by the magnetic behavior of the polycrystalline sample.

4.1.2 Measurements on $Lu_{0.1}Y_{0.9}Fe_2O_{4-\delta}$

I have prepared samples with a high percentage of Y i.e. $Lu_{0.1}Y_{0.9}Fe_2O_{4-\delta}$, because according to **[Kishi et al., 1983]**, this composition showed a magnetic behavior distinct from both $LuFe_2O_4$ and YFe_2O_4, so we expected a new charge and spin orders. Within the time frame of the practical part of this thesis work, only polycrystalline samples could be prepared,

and my magnetization measurements M(T) indicate that my sample quality has to be further improved, which could be done in the future.

A different magnetic behavior is noticed compared to YFe_2O_4, $Lu_{0.5}Y_{0.5}Fe_2O_4$ and Kishi's measurements. However, all comparisons are tentative, since no stoichiometric samples are available and it is necessary to examine if this YFe_2O_4 with the low Lu substitution exhibits distinct charge and spin orders from the pure compounds.

4.2 Recommendations for Future Work

For $Lu_{0.5}Y_{0.5}Fe_2O_4$, the biggest challenge for future work will be to grow single crystals with higher stoichiometry. It will be very interesting to investigate the CO of the stoichiometric crystal by single crystal X-ray diffraction, further to establish the magnetic phase diagram by magnetization measurements, and to study the spin order by neutron diffraction. However, for optimized $Lu_{0.5}Y_{0.5}Fe_2O_4$ we expect the same spin and charge orders as observed in $LuFe_2O_4$. The refinements of the CO crystal and magnetic structure are important, but it depends on the CO results since CO crystal and the magnetic structure of $LuFe_2O_4$ were already refined by **[de Groot et al. 1, 2012]**.

For the interesting composition $Lu_{0.1}Y_{0.9}Fe_2O_4$, the polycrystalline synthesis needs to be further optimized. For the optimized sample, again the same procedure used in the investigation of the CO and SO of $Lu_{0.5}Y_{0.5}Fe_2O_4$ may be repeated, since different structures are expected. To study these microscopically, it will be crucial to also obtain stoichiometric enough single crystals.

Studying the substitution of In for Lu in $LuFe_2O_4$ is even more interesting, as not much has been done in this region of the R^{3+} size, but also more challenging in regard of the synthesis as In has a relatively high vapor pressure, and for $InFe_2O_{4-\delta}$ no single crystals are currently available, and no partial substitution studies have been reported at all.

According to **[Oka et al., 2008]**, both the magnetic behavior and the CO for $InFe_2O_4$ are distinct from $LuFe_2O_4$. Starting with the solid state synthesis of $InFe_2O_4$, it is necessary to verify this, using the same mixed gas-flow as for $Lu_xY_{1-x}Fe_2O_{4-\delta}$ to fine-tune the stoichiometry and to avoid the Fe_3O_4 impurity they reported. A synthesis of polycrystalline $Lu_xIn_{1-x}Fe_2O_4$ and magnetic characterization is required to establish the compositional boundaries

between different ground states, as done in **[Kishi et al., 1983]** for $Lu_xY_{1-x}Fe_2O_4$. Finally, an ambition would be, to synthesize and optimize single crystals for the compositions selected according to the above, and to study these with the same methods as described for $Lu_xY_{1-x}Fe_2O_4$ to determine charge and spin order.

Investigation of the CO in the intercalated RFe_2O_4 is important, because the insertion of one or more blocks of $RFeO_3$ will modify the coupling between different bilayers. This will likely lead to new patterns of charge and spin order in the bilayers. It is also worth noting that the only believable polarization hysteresis loop in the rare earth ferrite literature **[Qin et al. 2, 2009]** was measured on an intercalated compound, slightly Mn-doped $Lu_2Fe_3O_7$. Very little has been done on intercalated compounds either experimentally or theoretically **[Qin et al. 1, 2009] and [Yang et al., 2010]**, mainly because of the absence of single crystalline specimens. $Lu_2Fe_3O_7$ showed superstructure reflections in electron diffraction up to higher temperatures than $LuFe_2O_4$ [**Yang et al., 2010**] although mixture of phases were observed in this work.

For the intercalated compounds, the first thing would be trying to reliably grow single crystals of $Lu_2Fe_3O_{7-\delta}$ as it was produced before as a secondary phase in the growth of $LuFe_2O_4$ crystals. Like for the substitution studies, the stoichiometry will then be fine-tuned to get stoichiometric single crystals, and finally one should investigate the spin and charge order by single crystal X-ray and neutron diffraction. To synthesize also intercalated compounds with other rare earth ferrites could be conducted, or one could investigate the effect of Mn-doping as done in **[Qin et al. 2, 2009] and [Qin et al. 1, 2009]** for polycrystalline samples.

Bibliography

[41st IFF Spring school, 2010]. 41st IFF Springschool. *Electronic Oxides – Correlation Phenomena, Exotic Phases and Novel Functionalities.* Jülich Forschungszentrum 13, 2010.

[Angst, 2013]. M. Angst. *Ferroelectricity from iron valence ordering in rare earth ferrites?*. Phys. Status Solidi RRL 7, 375 (2013).

[Angst, 2015]. M. Angst. Lecture notes: *Material analysis by synchrotron radiation and neutrons.* RWTH Aachen University, 2015.

[Angst et al., 2008]. M. Angst, R. P. Hermann, A. D. Christianson, M. D. Lumsden, C. Lee, M.-H. Whangbo, J.-W. Kim, P. J. Ryan, S. E. Nagler, W. Tian, et al.. *Charge Order in $LuFe_2O_4$: Antiferroelectric Ground State and Coupling to Magnetism*. Phys. Rev. Lett. 101, 227601 (2008).

[Angst, private communication]. M. Angst. *private communication*.

[Bibes and Barthélémy, 2008]. M. Bibes, and A. Barthélémy. *Multiferroics: Towards a magnetoelectric memory.* Nature materials 7, 425 (2008).

[Cao et al., 2012]. S. Cao, J. Li, Z. Wang, H. Tian, Y. Qin, L. Zeng, C. Ma, H. Yang & J. Li. *Extreme chemical sensitivity of nonlinear conductivity in charge-ordered $LuFe_2O_4$*. Sci. Rep. 2, 330 (2012).

[Christianson et al., 2008]. A. D. Christianson, M. D. Lumsden, M. Angst, Z. Yamani, W. Tian, R. Jin, E. A. Payzant, S. E. Nagler, B. C. Sales, & D. Mandrus. *Three-Dimensional Magnetic Correlations in Multiferroic $LuFe_2O_4$*. Phys. Rev. Lett. 100, 107601 (2008).

[de Groot, 2012]. J. de Groot. *Charge, spin and orbital order in the candidate multiferroic material $LuFe_2O_4$*. Ph.D. thesis, RWTH Aachen (2012).

[de Groot et al. 1, 2012]. J. de Groot, T. Mueller, R. A. Rosenberg, D. J. Keavney, Z. Islam, J.-W. Kim, & M. Angst. *Charge Order in $LuFe_2O_4$: An Unlikely Route to Ferroelectricity*. Phys. Rev. Lett. 108, 187601 (2012).

[de Groot et al. 2, 2012]. J. de Groot, K. Marty , M. D. Lumsden, A. D. Christianson, S. E. Nagler, S. Adiga, W. J. H. Borghols, K. Schmalzl, Z. Yamani, S. R. Bland, R. de Souza, U. Staub, W. Schweika, Y. Su, & M. Angst. *Competing Ferri- and Antiferromagnetic Phases in Geometrically Frustrated $LuFe_2O_4$* . Phys. Rev. Lett. 108, 037206 (2012).

[Dynacool user's manual]. RUL:
http://www.mrfn.org/sites/www.mrfn.org/files/instrument/DynaCool Manual_A0.pdf

[Eerenstein et al., 2006]. W. Eerenstein, N. D. Mathur, & J. F. Scott. *Multiferroic and magnetoelectric materials.* Nature 442, 759 (2006).

[Fiebig, 2005]. M. Fiebig. *Revival of the magnetoelectric effect*. Journal of Physics D: Applied Physics 38, R123 (2005).

[Hervieu et al., 2014]. M. Hervieu, A. Guesdon, J. Bourgeois, E. Elkaïm, M. Poienar, F. Damay, J. Rouquette, A. Maignan & C. Martin. *Oxygen storage capacity and structural flexibility of $LuFe_2O_{4+x}$ ($0 \leq x \leq 0.5$)*. Nature Mater. 13, 74 (2014).

[Hill, 2000]. N. A. Hill. *Why Are There so Few Magnetic Ferroelectrics?*. The Journal of Physical Chemistry B 104, 6694 (2000).

[ICSD website]. International Crystallographic Database. RUL: https://icsd.fiz-karlsruhe.de.

[Horibe et al., 2004]. Y. Horibe, K. Kishimoto, S. Mori, and N. Ikeda. *Dielectric Anomaly and Structural Phase Transitions in $YFe_2O_{4-\delta}$*. Integr. Ferroelectr. 67, 151 (2004).

[Iida et al., 1986]. J. Iida, Y. Nakagawa, and N. Kimizuka**.** *Field Heating Effect Anomalous Thermomagnetization Curves Observed in Hexagonal $LuFe_2O_4$***.** J. Phys. Soc. Jpn. 55,1434 (1986).

[Iida et al., 1990]. J. Iida, S. Takekawa, & N. Kimizuka. *Single crystal growth of $LuFe_2O_4$, $LuFeCoO_4$ and $YbFeMgO_4$ by the floating zone method*. J. Cryst. Growth 102, 398 (1990).

[Ikeda et al., 2005]. N. Ikeda, H. Ohsumi, K. Ohwada, K. Ishii, T. Inami, K. Kakurai, Y. Murakam, K. Yoshii, S. Mori, Y. Horibe, H. Kitˆo. *Ferroelectricity from iron valence ordering in the charge-frustrated system $LuFe_2O_4$*. Nature 436, 1136 (2005).

[Jacop and Rajitha, 2012]. K.T. Jacob, G. Rajitha. *Nonstoichiometry, defects and thermodynamic properties of $YFeO_3$, YFe_2O_4 and $Y_3Fe_5O_{12}$*. Solid State Ionics 224, 32 (2012).

[Inazumi et al., 1981]. M. Inazumi, Y. Nakagawa, M. Tanaka, N. Kimizuka, & K. Siratori. *Magnetizations and Mossbauer spectra of YFe_2O_{4-x}*. J. Phys. Soc. Jpn. 50, 438 (1981).

[Kitayama et al., 2004]. K. Kitayama, M. Sakaguchi, Y. Takahara, H. Endo, and H. Ueki. *Phase equilibrium in the system Y-Fe-O at 1100 ˚C*. J. Solid State Chem. 177, 1933 (2004).

[Khomskii, 2009]. D. Khomskii. *Classifying multiferroics: Mechanisms and effects*. Physics 2, 20 (2009).

[Kimizuka and Katsura 1, 1975]. N. Kimizuka and T. Katsura. *Standard free energy of formation of $YFeO_3$, $Y_3Fe_5O_{12}$, and a new compound YFe_2O_4 in the $Fe—Fe_2O_3—Y_2O_3$ system at 1200 ˚C*. J. Solid State Chem. 13, 176 (1975).

[Kimizuka and Katsura 2, 1975]. N. Kimizuka and T. Katsura. *The Standard Free Energy of Formation of $YbFe_2O_4$, $Yb_2Fe_3O_7$, $YbFeO_3$, and $Yb_3Fe_2O_{12}$ at 1200 ˚C*. J. Solid State Chem. 15,151-l 57 (1975).

[Kishi et al., 1983]. M. Kishi, Y. Nakagawa, M. Tanaka, N. Kimizuka, & I. Shindo. *Low-Temperature transitions of RFe_2O_4*. J. Magn. and Magn. Mater. 31-34, 807 (1983).

[Ko et al., 2009]. K.-T. Ko, H.-J. Noh, J.-Y. Kim, B.-G. Park, J.-H. Park, A. Tanaka, S. B. Kim, C. L. Zhang, & S-W. Cheong. *Electronic Origin of Giant Magnetic Anisotropy in Multiferroic $LuFe_2O_4$*. PRL 103, 207202 (2009).

[Kumar, 2012]. C. M. N. Kumar. *Crystal and spin structure and their realation to physical properties in some geometrical and spin spiral multiferroics.* Master thesis, **RWTH Aachen** (2012).

[Lafuerza et al., 2013]. S. Lafuerza, J. Garc´ıa, G. Sub´ıas, J. Blasco, K. Conder & E. Pomjakushina. *Intrinsic electrical properties of $LuFe_2O_4$*. Phys. Rev. B 88, 085130 (2013).

[Moessner and Ramirez, 2006]. R. Moessner and A. P. Ramirez. *Geometrical frustration*. Phys. Today 59(2), 24 (2006).

[Mueller, 2012]. T. Mueller. *Charge, spin and orbital order in highly stoichiometric $YFe_2O_{4-\delta}$ single crystals*. Diploma thesis, RWTH Aachen (2012).

[Mueller et al., 2015]. T. Mueller, J. de Groot, J. Strempfer, & M. Angst. *Stoichiometric $YFe_2O_{4-\delta}$ single crystals, grown by the optical floating-zone method.* J. Crystal Growth 428, 40 (2015).

[Mueller et al., unpublished]. T. Mueller. *unpublished*.

[Naka et al., 2008]. M. Naka, A. Nagano, & S. Ishihara**.** *Magnetodielectric phenomena in a charge- and spin-frustrated system of layered iron oxide*. Phys. Rev. B 77, 224441 (2008).

[Nakamura et al., 1998]. S. Nakamura, H. Kitˆo, & M. Tanaka. *An approach to specify the spin configuration in the RFe_2O_4 (R=Y, Ho, Er, Tm, Yb, and Lu) family: ^{57}Fe M¨ossbauer study on a single crystal $LuFe_2O_4$*. Journal of Alloys and Compounds 275-277, 574 (1998).

[Neutron lab course book, 2013]. Th. Brückel, G. Heger, D. Richter, G. Roth & R. Zorn. *Neutron Scattering*. Jülich Forschungszentrum 63, 2013**.**

[Niermann et al., 2012]. D. Niermann, F. Waschkowski, J. de Groot, M. Angst, & J. Hemberger. *Dielectric properties of charge ordered $LuFe_2O_4$ Revisited: The Apparent Influence of Contacts*. Phys. Rev. Lett. 109, 016405 (2012).

[Noh et al., 2010]. H. J. Noh, H. Sung, J. Jeong, J. Jeong, S. B. Kim, J. Y. Kim, J. Y. Kim, & B. K. Cho. *Effect of structural distortion on ferromagnetic order in $Lu_{1-x}L_xFe_2O_4$ (L=Y and Er; x=0.0, 0.1, and 0.5).* Phys. Rev. B 82, 024423 (2010).

[Oka et al., 2008]. K. Oka, M. Azuma, N. Hayashi, S. Muranaka, Y. Narumi, K. Kindo, S. Ayukawa, M. Kato, Y. Koike, Y. Shimakawa, & M. Tankano. *Charge and Magnetic Orderings in the Triangular-Lattice Antiferromagnet $InFe_2O_4$*. J. Phys. Soc. Jpn. 77, 064803 (2008).

[Qin et al. 1, 2009]. Y. B. Qin, H. X. Yang, Y. Zhang, H. F. Tian, C. Ma, Y. G. Zhao, R. I. Walton & J. Q. Li. *The effect of Mg doping on the structural and physical properties of $LuFe_2O_4$ and $Lu_2Fe_3O_7$*. J. Phys.: Condens. Matter 21, 015401 (2009).

[Qin et al. 2, 2009]. Y. B. Qin, H. X. Yang, Y. Zhang, H. F. Tian, C. Ma, L. J. Zeng, and J. Q. Li. *Suppression of the current leakage in charge ordered $Lu_2Fe_2Fe_{1-x}Mn_xO_7$ ($0 < x \leq 0.86$)*. Appl. Phys. Lett. 95, 072901 (2009).

[Roy et al., 2012]. A. Roy, R. Gupta, & A. Garg. *Multiferroics Memories.* Advances in Condensed Matter Physics, (2012).

[Ruff et al., 2012]. A. Ruff, S. Krohns, F. Schrettle, V. Tsurkan, P. Lunkenheimer, & A. Loidl. *Absence of polar order in $LuFe_2O_4$*. Eur. Phys. J. B 85, 290 (2012).

[Schmid, 2008]. H. Schmid. *Some symmetry aspects of ferroics and single phase multiferroics.* J. Phys.: Condens. Matter 20, 434201 (2008).

[Schrettle et al., 2011]. F. Schrettle, S. Krohns, P. Lunkenheimer, V. A. M. Brabers, & A. Loidl. *Relaxor ferroelectricity and the freezing of short-range polar order in magnetite*. Phys. Rev. B. 83, 195109 (2011).

[Sekine and Katsura, 1976]. T. Sekine & T. Katsura. *Phase Equilibria in the System Fe-Fe_2O_3-Lu_2O_3 at 1200 $^{\circ}C$*. Journal Of Solid State Chemistry 17, 49 (1976).

[Senn et al., 2012]. M. S. Senn, J. P. Wright, J.P. Attfield. *Charge order and three-site distortions in the Verwey structure of magnetite*. Nature 481, 173 (2012).

[Serrao et al., 2008]. C. R. Serrao, J. R. Sahu, K. Ramesha, & C. N. R. Rao. *Magnetoelectric effect in rare earth ferrites, $LnFe_2O_4$*. J. Appl. Phys. 104, 016102 (2008).

[Shindo et al., 1976]. I. Shindo, N. Kimizuka, & S. Kimura. *Growth of YFe_2O_4 single crystals by floating zone method*. Mater. Res. Bull. 11, 637 (1976).

[Sun et al., 2013]. Y. Sun, J.-Z. Cong, Y.-S. Chai, L.-Q. Yan, Y.-L. Zhao, S.-G. Wang, W. Ning, and Y.-H. Zhang. *Giant exchange bias in a single-phase magnet with two magnetic sublattices.* Appl. Phys. Lett. 102, 172406 (2013).

[Supernova User Manual, 2014]. Agilent Technologies. URL: http://www.agilent.com/cs/library/usermanuals/public/SuperNova_User_Manual.pdf

[Verwey, 1939]. E. J. W. Verwey. *Electronic Conduction of Magnetite (Fe_3O_4) and its Transition Point at Low Temperatures*. Nature 144, 327 (1939).

[Volger, 1954]. J. Volger. *Further experimental investigations on some ferromagnetic oxidic compounds of maganese with perovskite strucutre*. Physica 20, 49 (1954).

[Wang et al., 2009]. F. Wang, J. Kim, & Y. -J. Kim. *Spin-Glass behavior in $LuFe_2O_{4+\delta}$*. Phys. Rev. B, 80, 024419 (2009).

[Wang et al., 2013]. F. Wang, J. Kim, G. D. Gu, Y. Lee, S. Bae et al.. *Oxygen stoichiometry and magnetic properties of $LuFe_2O_{4+\delta}$*. J. Appl. Phys. 113, 063909 (2013).

[Williamson, 2012]. H. Williamson. *Magnetic and Charge Order in $LuFe_2O_4$ and $YbFe_2O_4$ Multiferroics***.** Master thesis, The University of Warwick (2012).

[Williamson et al., unpublished]. H. Williamson. *unpublished*.

[Wu et al., 2008]. W. Wu, V. Kiryukhin, H.-J. Noh, K.-T. Ko, J.-H. Park, W. Ratcliff, P. A. Sharma, N. Harrison, Y. J. Choi, Y. Horibe, S. Lee, S. Park, H. T. Yi, C. L. Zhang, & S.-W. Cheong.

Formation of Pancakelike Ising Domains and Giant Magnetic Coercivity in Ferrimagnetic $LuFe_2O_4$. Phys. Rev. Lett. 101, 137203 (2008).

[Xiang and Whangbo, 2007]. H. J. Xiang & M.-H. Whangbo. *Charge Order and the Origin of Giant Magnetocapacitance in $LuFe_2O_4$*. PRL 98, 246403 (2007).

[Xiang et al., 2009]. H. J. Xiang, E. J. Kan, S.-H. Wei, M.-H. Whangbo, & J. Yang. *Origin of the Ising ferrimagnetism and spin-charge coupling in $LuFe_2O_4$*. Phys. Rev. B 80, 132408 (2009).

[Yamada et al., 2000]. Y. Yamada, K. Kitsuda, S. Nohdo, & N. Ikeda. *Charge and spin ordering process in the mixed-valence system $LuFe_2O_4$: Charge ordering*. Phys. Rev. B 62, 12167 (2000).

[Yang et al., 2010] H. Yang, Y. Zhang, Y. Qin, C. Ma, H. Tian, & J. Li. *Electronic ferroelectricity, charge ordering and structural phase transitions in $LuFe_2O_4(LuFeO_3)_n$ (n = 0 and 1)*. Phys. Status Solidi B 247, 870 (2010).

[Yoshii et al., 2008]. K. Yoshii, Y. Yoneda, D. Maeda, Y. Yokota, T. Michiuchi, T. Komatsu, N. Ikeda, Y. Matsuo, & S. Mori. *Magnetic and Dielectric Properties of $HoFe_2O_4$ and $R_{1-x}R_xFe_2O_4$ (R, R: Rare Earths)*. Japanese Journal of Applied Physics, 47, No. 9, 7599 (2008).

[Yoshii et al., 2012]. K. Yoshii, N. Ikeda, Y. Nishihata, D. Maeda, R. Fukuyama, T. Nagata, J. Kano, T. Kambe, Y. Horibe & S. Mori. *Exchange Bias in Multiferroic RFe_2O_4 (R = Y, Er, Tm, Yb, Lu, and In)*. Journal of the Physical Society of Japan 81, 033704 (2012).

تأثير تغير حجم أيون العناصر الأرضية النادرة على ترتيب الشحنات في مركبات RFe_2O_4

اعداد: صابرين حمودة

اشراف:
الدكتور سلمان محمد سلمان
والدكتور مانويل انغست

الملخص

تم في هذا البحث دراسة تأثير تغير حجم أيون العناصر الأرضية النادرة على ترتيب الشحنات في مركبات RFe_2O_4 وذلك عن طريق التهجين والاستبدال في المركب $Lu_xY_{1-x}Fe_2O_4$ للعنصر Y بنسبة مولية $x-1$ بدلا من الذرة الأصلية Lu.

تم اختيار المركب المهجن $Lu_{0.5}Y_{0.5}Fe_2O_4$ بنسبة استبدال 50% وذلك لأنه اظهر سلوكا مغناطيسيا مماثلا للسلوك المغناطيسي للمركب غير المهجن $LuFe_2O_4$ وبالتالي توقعنا ترتيب شحنات مماثل له. بينما تم اختيار $Lu_{0.1}Y_{0.9}Fe_2O_4$ لأنه أظهر سلوكا مغناطيسيا مختلفا تماما عن المركبين غير المهجنين والمحتويين على أحد العنصرين فقط رغم احتوائه نسبة 90% من Y. وتوقعنا لذلك ترتيب شحنات مختلف يعكس السلوك المغناطيسي المختلف.

وبالأخذ بالاعتبار أن نقص النسبة المولية المعيارية للأكسجين في المركب يؤثر على ترتيب الشحنات فقد تم تصنيع أكثر من عينة مسحوق المركب تحت تدفق من غاز CO_2-H_2 (4%)/Ar (96%) بالضغط الجزئي للأكسجين الذي يوثر على كمية الأكسجين المتوافرة.

وقد تم قياس التوزيع الاستبدالي لعينات مسحوق المركب المهجن الأول $Lu_{0.5}Y_{0.5}Fe_2O_4$ والمصنعة تحت تدفقات مختلفة من الغاز وبالتالي الأكسجين باستعمال الأشعة السينية. ومن ثم تمت

دراسة السلوك المغناطيسي بدلالة نسبة الأكسجين باستخدام جهاز PPMS. وفوق هذا استعمال تقنية TGA لحساب النقص في نسبة الأكسجين لبعض العينات. وتم تصنيع بلورات منفردة باستعمال تقنية OFZ تحت تدفق من غاز CO_2–CO بنسب مختلفة للحصول على بلورات بكمية مشبعة من نسبة الأكسجين المعيارية, وأخيرا تم فحص ترتيب الشحنات في البلورات عن طريق تحليل الأشعة السينية.

وقد تم اختيار افضل عينة سلوك مغناطيسي من مسحوق $Lu_{0.5}Y_{0.5}Fe_2O_4$ مما يعكس توفر نسبة الأكسجين الأقرب للمعيارية فيها. وقد تشابه السلوك المغناطيسي لهذه العينة بشكل كبير مع المركب النقي $LuFe_2O_4$. وأشارت القياسات المغناطيسية إلى تواجد ترتيبين مغناطيسين متنافسين AFM–fM بالضبط كما الحال في $LuFe_2O_4$. بالمقابل لم تظهر البلورات المصنعة لنفس المركب المهجن سلوكا مغناطيسيا مناظرا كما حال المسحوق. ولم تظهر ترتيبا للشحنات إلا ببعدين فقط مما يدل على عدم تحقق نسبة الأكسجين المعيارية للبلورات مقارنة بالمسحوق.

أما المركب المهجن الآخر $Lu_{0.1}Y_{0.9}Fe_2O_4$ فقد تم إنتاج عينات مسحوق فقط وتحت ظروف نسب أكسجين مختلفة قرب المعيارية كما الحال في المركب الأول. وقد أظهر قياس سلوكها المغناطيسي اختلافا واضحا عن أي من المركبين غير المهجنين $LuFe_2O_4$, YFe_2O_4, أو المركب المهجن السابق $Lu_{0.5}Y_{0.5}Fe_2O$. مما يطرح أسئلة عن كون سبب ذلك مرتبط بسوء تشكل العينات أو ربما تغير السلوك لظهور حالات تحول مغناطيسي مما يتطلب المزيد من الدراسة والتدقيق.

بخصوص المركب المهجن الأول $Lu_{0.5}Y_{0.5}Fe_2O_4$ أوصي ببناء بلورات بظروف اكثر معيارية لتوفر الأكسجين ومن ثم دراسة ترتيب الشحنات بتحليل تشتت الأشعة السينية والترتيب المغناطيسي بتحليل تشتت النيوترونات. وبخصوص المركب المهجن الآخر $Lu_{0.1}Y_{0.9}Fe_2O_4$ اقترح إعادة الدراسة بشكل كامل والتركيز على تصنيع مسحوق معياري وبلورات مشبعة أيضا لمعرفة مصدر السلوك المغناطيسي المختلف.